Title	State-space modelling of the flight behaviour of a soaring bird provides new insights to migratory strategies
Author(s)	Pirotta, Enrico; Katzner, Todd; Miller, Tricia A.; Duerr, Adam E.; Braham, Melissa A.; New, Leslie
Publication date	2018-06-09
Original citation	Pirotta, E., Katzner, T., Miller, T. A., Duerr, A. E., Braham, M. A. and New, L. (2018) 'State-space modelling of the flight behaviour of a soaring bird provides new insights to migratory strategies', Functional Ecology. doi:10.1111/1365-2435.13180
Type of publication	Article (peer-reviewed)
Link to publisher's version	http://dx.doi.org/10.1111/1365-2435.13180 Access to the full text of the published version may require a subscription.
Rights	**© 2018, the Authors. Functional Ecology © British Ecological Society. Published by John Wiley & Sons Inc. This is the peer reviewed version of the following article: Pirotta, E., Katzner, T., Miller, T. A., Duerr, A. E., Braham, M. A. and New, L. (2018) 'State-space modelling of the flight behaviour of a soaring bird provides new insights to migratory strategies', Functional Ecology. doi:10.1111/1365-2435.13180, which has been published in final form at https://doi.org/10.1111/1365-2435.13180. This article may be used for non-commercial purposes in accordance with Wiley Terms and Conditions for Use of Self-Archived Versions.**
Embargo information	Access to this article is restricted until 12 months after publication by request of the publisher.
Embargo lift date	2019-06-09
Item downloaded from	http://hdl.handle.net/10468/6599

State-space modelling of the flight behaviour of a soaring bird provides new

insights to migratory strategies

Enrico Pirotta[a,b]*, Todd Katzner[c], Tricia A. Miller[d], Adam E. Duerr[e], Melissa A. Braham[f], and

Leslie New[a]

[a] Department of Mathematics and Statistics, Washington State University, Vancouver, WA, USA

[b] School of Biological, Earth & Environmental, Sciences, University College Cork, Distillery

Fields, North Mall, Cork, Ireland

[c] U.S. Geological Survey, Forest & Rangeland Ecosystem Science Center, Boise, ID, USA

[d] Conservation Science Global, West Cape May, NJ, USA

[e] Bloom Biological Inc., Santa Ana, CA, USA

[f] Division of Forestry & Natural Resources, West Virginia University, Morgantown, WV, USA

*Corresponding author: enrico.pirotta@wsu.edu

Abstract

1. Characterizing the spatiotemporal variation of animal behaviour can elucidate the way individuals interact with their environment and allocate energy. Increasing sophistication of tracking technologies paired with novel analytical approaches allows the characterisation of movement dynamics even when an individual is not directly observable.

2. In this study, high-resolution movement data collected via global positioning system (GPS) tracking in three dimensions were paired with topographical information and used in a Bayesian state-space model to describe the flight modes of migrating golden eagles (*Aquila chrysaetos*) in eastern North America.

3. Our model identified five functional behavioural states, two of which were previously undescribed variations on thermal soaring. The other states comprised gliding, perching and orographic soaring. States were discriminated by movement features in the horizontal (step length and turning angle) and vertical (change in altitude) planes, and by the association with ridgelines promoting wind deflection. Tracked eagles spent 2%, 31%, 38%, 9% and 20% of their day time in directed thermal soaring, gliding, convoluted thermal soaring, perching and orographic soaring, respectively. The analysis of the relative occurrence of these flight modes highlighted yearly, seasonal, age, individual and sex differences in flight strategy and performance. Particularly, less energy-efficient orographic soaring was more frequent in autumn, when thermals were less available. Adult birds were also better at optimising energy efficiency than sub-adults.

4. Our approach represents the first example of a state-space model for bird flight mode using altitude data in conjunction with horizontal locations, and is applicable to other

39   flying organisms where similar data are available. The ability to describe animal

40   movements in a three-dimensional habitat is critical to advance our understanding of the

41   functional processes driving animals' decisions.

42   **Keywords:** 3D states, GPS-GSM telemetry, hidden state model, Markov chain Monte Carlo,

43   movement ecology, raptor, subsidised flight

44

45   **Introduction**

46   The way in which animals move in space and over time has important implications on their vital

47   rates and, ultimately, their fitness and demography (Nathan et al., 2008). Different movement

48   modes often require varying levels of energy expenditure and may reflect different

49   environmental constraints (Shepard et al., 2013). Understanding movement dynamics and

50   characterising the way in which they combine into functional bouts of activity can therefore help

51   formulate hypotheses regarding movement drivers, environmental influences, and energetic and

52   fitness implications of different behavioural strategies (Hays et al., 2016; Nathan et al., 2008).

53   Movement behaviour is difficult to observe directly for prolonged periods, especially for species

54   that range over large distances and move through media that are mostly inaccessible to human

55   observers (air or water). Recent advances in bio-logging technology allow tracking individuals

56   over wide spatiotemporal ranges and in remote areas, opening windows on their life history at

57   functionally relevant scales (Hays et al., 2016; Kays, Crofoot, Jetz, & Wikelski, 2015).

58   Telemetry data collection was originally aimed at tracking an animal's geographical location.

59   However, the proliferation of devices capable of collecting and storing information at fine

60   temporal resolutions, combined with the refinement of statistical tools, means that these data can

61 also be used to infer the behavioural patterns of tagged animals (Jonsen et al., 2013; Langrock et

62 al., 2012; McClintock, Russell, Matthiopoulos, & King, 2013; Patterson, Thomas, Wilcox,

63 Ovaskainen, & Matthiopoulos, 2008).

64 While various techniques have been proposed for the classification of behaviour, hidden state

65 models offer several advantages, particularly because they explicitly account for the intrinsic

66 autocorrelation of movement data (Jonsen et al., 2013; Langrock et al., 2012; McClintock et al.,

67 2012). These approaches assume that observed movement metrics arise from distributions that

68 depend on a latent sequence of discrete behavioural states or modes (known as emission

69 distributions), and are thus consistent with the often unobservable nature of behaviour. State

70 assignment is directly informed by the data, which can guide behavioural classification, reveal

71 unexpected patterns and thus lead to a new understanding of behaviour. State-space models,

72 which constitute a class of hidden state models, also allow accounting for any measurement error

73 associated with observed metrics (Jonsen et al., 2013; Patterson et al., 2008). This occurs

74 because they are composed of a process model, capturing the underlying transition between

75 states, and an observation model, describing the way in which data are generated, with error.

76 Most classic developments and applications of movement models have focused on the marine

77 realm (e.g., marine mammals, seabirds, elasmobranchs or large teleosts, see references in Jonsen

78 et al., 2013) or on terrestrial non-volant mammals (e.g. Morales, Haydon, Frair, Holsinger, &

79 Fryxell, 2004). The main objective of these studies has been distinguishing between two

80 behavioural modes: periods where an individual rapidly moves through unprofitable areas or

81 travel corridors (transit mode), and periods where it explores an area in search of patchy food

82 resources (resident mode) (Jonsen et al., 2013; Morales et al., 2004; Patterson et al., 2008).

83   Recently, important progress has been made in finer discrimination of behaviour by providing

84   additional data streams to inform the models, characterizing, for example, attraction to specific

85   locations (McClintock et al., 2012), central place foraging (Michelot et al., 2017; Pirotta,

86   Edwards, New, & Thompson, 2018), diving (Bestley, Jonsen, Hindell, Harcourt, & Gales, 2015;

87   Dean et al., 2013; Isojunno & Miller, 2015; Quick et al., 2017), and active foraging (Isojunno &

88   Miller, 2015).

89   Few existing applications of hidden state models describe the behaviour of terrestrial birds

90   (Leos-Barajas et al., 2017; Péron et al., 2017; Williams, Shepard, Duriez, & Lambertucci, 2015).

91   For these species, characterising flight modes may be more relevant than distinguishing between

92   transit and resident movement, because of the implications on their energy budget. Such

93   characterisation requires either the use of additional sensors, like accelerometers, or the

94   introduction of a third movement dimension (altitude), which is conceptually comparable to the

95   use of depth when modelling diving behaviour of marine animals (Isojunno & Miller, 2015;

96   Quick et al., 2017). Birds adopt different strategies to move through air, depending on their size,

97   body structure, reasons for moving, and environmental and weather conditions (Duerr et al.,

98   2015; Hedenstrom, 1993; Lanzone et al., 2012). Flapping flight is costly, and heavier species

99   tend to soar (i.e. use air currents to support straight-winged flight) as a more efficient way to

100 move over large distances (Hedenström & Alerstam, 1995). Broadly speaking, there are two

101 predominant soaring modes in terrestrial birds. Thermal soaring is defined as the use of thermals

102 (i.e. layers of warm air that rise from the earth forming updrafts) to gain altitude, followed by

103 periods of gliding towards other thermals to continue their progression. Conversely, orographic

104 soaring relies on horizontal winds deflected upwards by ridges, trees, hills and other structures

105 (Duerr et al., 2015; Kerlinger, 1989).

5

106   In this study, a large telemetry dataset from golden eagles (*Aquila chrysaetos*) in eastern North

107   America was used to develop a Bayesian state-space model describing the flight behaviour of

108   soaring birds. These birds are from a small population of approximately 5,000 individuals

109   migrating between the breeding grounds in Canada and a wintering range in the northern and

110   central Appalachian Mountains and surrounding regions (Dennhardt, Duerr, Brandes, & Katzner,

111   2015; Katzner, Smith, et al., 2012). The population faces increasing pressure from wind power

112   development in the southern part of its range and along its migratory route, which has sparked

113   research on the factors influencing individuals' risk of colliding with turbines (Katzner, Brandes,

114   et al., 2012; Miller et al., 2014). The choice of different flight modes by these birds changes their

115   altitude, speed and updraft use and, although it is likely to contribute to collision risk, is rarely

116   accounted for when predicting fatality rates (Barrios & Rodríguez, 2004; Klaassen, Strandberg,

117   Hake, & Alerstam, 2008).

118   Golden eagles use both thermal and orographic soaring to maximise flight efficiency under

119   different weather and environmental conditions (Duerr et al., 2012; Katzner et al., 2015; Lanzone

120   et al., 2012). Therefore, they represent an ideal system for the development of a model to

121   categorise flight modes, which could be easily applicable to other flying organisms. Below, the

122   modelling framework is presented and utilized to characterise a high-resolution time series of

123   golden eagle behaviour using location and altitude information collected via GPS, together with

124   ancillary environmental data. The behavioural results are then analysed to investigate the activity

125   budget of eagles belonging to different age and sex classes in different seasons, and to explore

126   the functional mechanisms underpinning individual flight performance during migration.

127

Materials and methods

129 *Data collection*

130 We used existing golden eagle telemetry data collected between 2009 and 2016 (Duerr et al.,

131 2012; Katzner et al., 2015; Miller et al., 2014). Eagles were captured and outfitted with CTT-

132 1100 GPS-GSM telemetry systems (Cellular Tracking Technologies, LLC) attached as

133 backpacks with Teflon™ ribbon (Bally Ribbon Mills in Bally, PA). Tags were programmed to

134 record location and altitude above sea level (calculated as height above the geoid) every 30-60

135 seconds from sunrise to sunset. No locations were recorded at night. The GPS device measured

136 instantaneous speed. If speed was less than 1 knot for 5 min, the unit switched to sampling data

137 at 15-min intervals, thus conserving battery power and device memory when a bird was

138 perching. Full details of the study area, deployment techniques, duty cycles, sampling regimes

139 and permits are reported in Katzner et al. (2015) and Miller et al. (2014, 2016). For the current

140 study, a total of 58 tracks were used, 48 of which were collected during the spring migration, and

141 10 in autumn (Fig. 1). Tagged eagles included juveniles (1st year of northbound migration, 8

142 tracks), sub-adults (2nd–4th year of migration, 22 tracks), and adults (>4th year of migration, 28

143 tracks). Nineteen tracks were from female individuals and 39 from males. Some individuals were

144 tracked over multiple years (Table S1 in Supporting information).

145 *Data processing*

146 Fixes with a horizontal dilution of precision (an indication of 2D location quality; HDOP) > 10

147 and 2D fixes were removed to exclude any obvious error in GPS locations or altitudes. Vertical

148 dilution of precision (VDOP) information was not available for the majority of the data. Due to

149   the sampling regime, there were gaps in the recorded tracks. Gaps in flight data could also have

150   occurred because of low battery voltage or the system's functionality. Furthermore, a unit could

151   not collect and send data simultaneously so, if a bird was in flight and connected to the Global

152   System for Mobile communications (GSM) network, GPS data were not collected. Therefore, to

153   reduce extrapolation over long unobserved periods, tracks from individual eagles were split into

154   separate segments whenever the interval between consecutive locations was greater than 5

155   minutes. Segments shorter than 10 minutes were excluded from further analysis to avoid biasing

156   the probabilities regulating the temporal sequence of states (see below). Because hidden state

157   models require a regular sampling unit, location and altitude data were linearly interpolated in R

158   with custom code to a constant one-minute temporal resolution (R Development Core Team,

159   2016). In alternative to using the interpolated values of the response variables over remaining

160   short ($\leq$ 5 min) unobserved periods in the data, the model can be formulated to estimate the value

161   of missing observations. Results of this reformulation are shown in Appendix S3.

162   At each minute, t, four variables were derived to characterise eagle behaviour (Table S2). The

163   use of these variables for describing the behaviour of soaring birds was supported by previous

164   studies (Katzner et al., 2015). Three of the four were derived from the GPS data: step length x_t

165   (the distance between location at t and location at $t + 1$, in meters), turning angle θ_t (the angle

166   between the step from $t - 1$ to t and the step from t to $t + 1$, in radians) and altitude above sea

167   level a_t (recorded by the GPS device, in meters). The fourth variable was hierarchical slope

168   position (HSP, as defined by Murphy, Evans & Storfer 2010), a metric of topographic

169   morphology used to quantify exposure and identify ridges. HSP was computed using package

170   spatialEco in R (Evans, 2017) and based on ground elevation data obtained from the Global

171   Multi-resolution Terrain Elevation Data 2010 at 30-arc-second spatial resolution (data available

8

172   from the U.S. Geological Survey: https://earthexplorer.usgs.gov/). A value of HSP, h_t, was

173   extracted for the surface below each eagle location at time t. These four variables constituted the

174   vector of behavioural observations $\mathbf{y}_t$. Because the calculation of the turning angle θ_t requires

175   three consecutive locations, the first and last locations of each segment were discarded.

176   We assumed that the error around GPS locations was negligible (Morales et al., 2004). This was

177   supported by the low mean HDOP associated with retained GPS fixes (mean = 1.9; STD = 1.2),

178   corresponding to location errors in the order of a few meters. Particularly, the standard deviation

179   of the position can be approximated by multiplying HDOP by the measurement standard

180   deviation of the GPS device (Poessel, Duerr, Hall, Braham, & Katzner, 2018), which was 3 m for

181   the devices used in this study (resulting in a standard deviation of 30 m when HDOP = 10).

182   Considering the distribution of step lengths for tagged animals (mean = 540 m; STD = 398 m),

183   this error was deemed irrelevant for our application. We used the published accuracy of the

184   device in the third dimension to inform the error around altitude measurements in a state-space

185   modelling framework (see details below; Lanzone et al., 2012).

186   We tested the use of altitude above ground level for the vertical dimension, but found models

187   with this variable to perform much worse than those with altitude above sea level. This was

188   possibly due to error propagation (Péron et al., 2017) or to the fact that altitude above ground

189   becomes difficult to interpret over steeply changing slopes, such as the ones used during

190   orographic flight (Katzner et al., 2015).

191   *Model structure*

192   We developed a Bayesian state-space model to estimate the time series of latent behavioural

193   states, s_t, of tagged individuals, together with the state-specific parameters of the emission

194   distributions for the observations $\mathbf{y}_t$. The process component of the model described the

195   transition between the underlying states, regulated by a matrix of transition probabilities $\mathbf{\Gamma}$. For

196   M states, $\mathbf{\Gamma}$ had dimensions $M \times M$ and each element $\gamma_{i,j}$ indicated the probability of being in state

197   j at time t, given that the animal was in state i at time $t - 1$. The Markov property was assumed

198   for the time series of states, i.e. state at time t only depended on state at time $t - 1$. The state

199   process was informed by the four variables, step length, turning angle, altitude and hierarchical

200   slope position, at time t. Given state $s_t = i$ (with i in $1,\ldots,M$), step lengths were modelled as

201   emerging from a Weibull distribution (McClintock et al., 2012; Morales et al., 2004), with state-

202   specific scale (α_i) and shape (β_i) parameters, determining the average step length per state and its

203   variability, i.e. $x_t \sim W(\beta_i, \alpha_i)$. Turning angles were assumed to have a wrapped Cauchy

204   distribution (McClintock et al., 2012; Morales et al., 2004) with mean (μ) equal to 0 and state-

205   specific concentration parameter (ρ_i), a measure of how angles are distributed around the mean,

206   i.e. $\theta_t \sim wC(0, \rho_i)$ (Breed, Costa, Jonsen, Robinson, & Mills-Flemming, 2012). The parameter ρ_i

207   varies between 1 (angles concentrated around the mean 0, i.e. directed movement) and 0

208   (corresponding to directions uniformly distributed on the circle, i.e. a classic random walk

209   allowing for convoluted movement). True, unobserved altitude at each minute t was modelled as

210   a random walk Gaussian variable with state-dependent standard deviation σ_i (Isojunno & Miller,

211   2015; Langrock, Marques, Baird, & Thomas, 2014), $v_t \sim N(v_{t-1} + \pi_i, \sigma_i)$, where v_{t-1} is the true

212   altitude in the previous minute and π_i denotes the state-specific mean vertical drift, i.e. the

213   change in altitude between minutes. A Gaussian observation model accounted for errors in

214   altitude measurement, i.e. $a_t \sim N(v_t, \varepsilon)$. Finally, following data exploration, hierarchical slope

215   position was assumed to emerge from a Gaussian distribution with state-specific mean κ_i and

216   standard deviation ω_i, i.e. $h_t \sim N(\kappa_i, \omega_i)$.

217 We tested several alternative structures for the model, including a range of potential latent states

218 (three to six). A model with five states converged successfully and aligned with biological

219 expectations, so only this parameterisation is presented here. It is important to note that, in an

220 unsupervised inference setting such as this (i.e. one where the true states are unknown), the

221 number of states is driven by the process generating observed data (Leos-Barajas et al., 2017).

222 However, the use of appropriate movement and ancillary environmental variables, capturing

223 relevant features of an animal's behaviour, can lead to the identification of biologically

224 meaningful latent states (Leos-Barajas et al., 2017; McClintock et al., 2013). The five states used

225 here were characterised by features of the response variables that broadly corresponded to

226 directed thermal soaring (state 1), gliding (state 2), convoluted thermal soaring (state 3), perching

227 (or on the ground; state 4) and orographic soaring (but potentially including periods of flapping

228 flight; state 5).

229 *Priors*

230 Following initial data exploration, a set of constraints was applied to the priors of state-specific

231 parameters in order to facilitate model convergence and support the identification and

232 assignment of functionally relevant latent states (Isojunno & Miller, 2015) (Appendix S1). This

233 also prevented label switching, i.e. the non-identifiability of state-dependent components due to

234 the posterior distribution being invariant to permutation of state labels (Stephens, 2000). These

235 constraints were broad, and were only defining the overall tendency of the vertical movement

236 (ascending, descending or stable overall) and the relative degree of directedness, speed and

237 topographic exposure among states (Appendix S1). The standard deviation of the observation

238   model for altitude (ε) was set at a fixed value (25 m), but was large enough to conservatively

239   account for the declared accuracy level (Lanzone et al., 2012).

240   *Model fitting*

241   The model was fitted using JAGS run from R (package runjags; Appendix S2) (Denwood, 2016).

242   Markov chain Monte Carlo (MCMC) algorithms were iterated until convergence of the latent

243   states and model parameters. State convergence was assessed by monitoring the proportion $\delta_{1,...,5}$

244   of minutes classified under each latent state. We ran three parallel chains, starting at different

245   initial values. Convergence was assessed by visually inspecting trace and density plots (Lunn,

246   Jackson, Best, Thomas, & Spiegelhalter, 2013), and confirmed by checking that the Brooks-

247   Gelman-Rubin (BGR) diagnostic fell below 1.1, and that Monte Carlo (MC) error was less than

248   5% of the sample standard deviation (Lunn et al., 2013). The R package coda was used to assess

249   convergence, calculate effective sample size and extract posterior estimates (Plummer, Best,

250   Cowles, & Vines, 2006).

251   *Model validation*

252   To investigate the model's ability to characterise functional latent states, we compared the

253   model's posterior state classifications with existing manual behavioural classifications for a

254   subset of tagged eagles. Particularly, data from 13 of the 48 spring tracks were previously

255   evaluated manually as part of a prior study (Katzner et al., 2015). Flight modes were identified

256   by an expert observer (T. A. Miller) based on the patterns of sequential GPS locations and on

257   their overlap with topographical features. As a result, flight mode was classified into one of four

258   states: thermal soaring, gliding, orographic soaring, and unknown (Katzner et al., 2015). Model

259   state classifications were obtained from the posterior median estimate of the categorical state.

260   States 1 and 3 were combined and matched to manually-classified thermal soaring, state 2 was

261   matched to manually-classified gliding, and state 5 to manually-classified orographic soaring.

262   Manual and model classifications were compared using confusion matrices. Because the model

263   could not assign an "unknown" state and accuracy could not be evaluated for "unknown"

264   segments, accuracy estimates from this matrix will be artificially low. In addition, we tested

265   whether the occurrence of gaps in the tracking data and measurement error in the horizontal and

266   vertical dimension could affect the results, using a simulation procedure based on the posterior

267   estimates of model parameters (Appendix S4) and carried out posterior predictive checks to

268   assess the goodness-of-fit of the model to the data (Appendix S5).

269   *Behavioural models*

270   The results of the state-space model can be used to explore the ecology of the study species. To

271   demonstrate this application, we carried out a descriptive investigation of the seasonal, age and

272   sex differences in flight strategy and performance. Specifically, we fitted binomial mixed-effects

273   models (package lme4 in R; Bates, Maechler & Bolker 2012) to test whether the proportional

274   occurrence of each behavioural state (directed thermal soaring, convoluted thermal soaring,

275   gliding and orographic soaring) in a track varied as a function of the interaction between season

276   (autumn and spring) and age category (adults and sub-adults). Because this analysis aimed to

277   compare the occurrence of flight modes, steps classified as on the ground or perching were

278   excluded. Moreover, due to the small sample size, tracks of juveniles were also excluded. In a

279   separate model, we tested for the effect of sex on the flight performance of adult eagles in the

280   two seasons (we excluded sub-adults since most of them were males). Because individuals were

281   tracked over multiple years, we included a random effect of individual and year in all models.

282   The random effects structure, as well as the inclusion of the fixed effects, was assessed using the

283   Akaike's information criterion (Gurka, 2006), corrected for small sample sizes (AICc).

284

285   **Results**

286   The 58 filtered eagle tracks corresponded to 72,844 GPS fixes, which made up 599 segments

287   longer than 10 min and separated from one another by more than 5 min. Regularisation of the

288   599 segments at a one-minute resolution reduced the sample analysed to 45,914 locations.

289   *State-space model*

290   Visual inspection of trace plots suggested that the chains were randomly oscillating around a

291   central value after 5,000 iterations, so these initial draws were discarded as burn-in. Diagnostics

292   confirmed that the model converged adequately after 15,000 iterations (Table S3). We also

293   verified that these iterations corresponded to an effective size of the posterior sample greater than

294   400 for all parameters (Lunn et al., 2013). Due to computing memory limitations, we only

295   retained one in 10 iterations.

296   The results were consistent with our biological expectations of eagle behaviour, embedded in the

297   priors, while describing the features of each state precisely. Under state 1 (directed thermal

298   soaring), an individual gained substantial altitude and moved in large, directed steps. State 3

299   (convoluted thermal soaring) was similar to state 1, but steps were considerably shorter and

300   turning angles had low concentration. Bouts of both states appeared to be followed by gliding

301   periods (state 2). State 4 (on the ground or perching) was characterised by extremely small and

302   convoluted horizontal steps, and visual investigation of the tracks confirmed it corresponded to

303 periods when an eagle was not moving (e.g. Fig. S2). Finally, state 5 (orographic soaring)

304 showed large variation in the vertical drift, suggesting irregular gaining and losing of altitude.

305 This flight mode was correctly classified to occur over topographies characterised by high

306 exposure (such as ridgelines). The posterior distributions of the state-dependent parameters are

307 summarised in Table S3 and the emission distributions of the four response variables (step

308 length, turning angle, vertical drift and hierarchical slope position) are plotted in Fig. S1.

309 The posterior median was used to classify the behavioural state at each time step. The

310 comparison of model state classifications with manually classified flight modes returned a mean

311 of 68% correct classifications across states (Table S4; 67% for thermal soaring, 70% for gliding

312 and 65% for orographic soaring). As an example, we plotted four track segments coloured by

313 state, where posterior true altitude values were used (Fig. 2). Based on posterior state

314 classifications, we calculated eagles' activity budget, across both migration seasons and by

315 migration season (Table 1). These data suggested that orographic soaring was less frequent in

316 spring than in autumn.

317 The model also appeared to be robust to observed levels of sampling irregularity and

318 measurement errors (Appendix S4). However, the posterior predictive checks highlighted

319 potential issues with the validity of the Markov property given the small time interval between

320 observations (Appendix S5, Figs. S4 and S5).

321 *Behavioural models*

322 Model selection highlighted differences among individuals and among years in the occurrence of

323 most flight modes (Table S5; Fig. S3). The use of orographic soaring varied by age category and

324 season, suggesting that this flight mode occurred proportionally more in autumn and was used

15

325   more by sub-adults (Fig. 3a). In contrast, directed thermal soaring occurred more in spring and

326   was used more by adults (Fig. 3a). Convoluted thermal soaring appeared to be used more by sub-

327   adults in autumn and by adults in spring, but the estimated effects had wide confidence intervals

328   (Fig. 3a). Gliding occurred more in spring, and was used more by adults, although the latter

329   effect showed large confidence intervals (Fig. 3a). Model results also suggested that the

330   proportional occurrence of orographic soaring and gliding varied between the sexes, but

331   differently in the two seasons. Females used more orographic soaring and less gliding than

332   males, but only in autumn (Fig. 3b). No difference between the sexes was found for directed or

333   convoluted thermal soaring (Table S5).

334

335   **Discussion**

336   To our knowledge, this study represents the first example of the use of altitude measurements in

337   conjunction with horizontal information and ancillary environmental variables in hidden state

338   models to characterise functional behavioural modes in three dimensions (McClintock, London,

339   Cameron, & Boveng, 2017; McClintock et al., 2013). This is particularly useful for flying

340   organisms, where studying the variation in flight mode might be more relevant than simply

341   distinguishing resident and transit movement identified by models in two dimensions (Jonsen et

342   al., 2013). In addition to identifying expected behavioural states of golden eagles, our model was

343   able to tease apart two types of thermal soaring with different directedness. Previous work has

344   generally classified thermal soaring as a single category of behaviour (e.g. Katzner et al., 2015),

345   while the combination of horizontal and vertical information in our study discriminated

346   additional flight features. The degree of directedness while gaining altitude within a thermal is

16

347   likely dependent upon the strength and distribution of thermals, the alignment of thermals with

348   flight direction, and wind conditions (Kerlinger, 1989). Whenever conditions cause thermals to

349   drift, birds using this form of soaring will also drift, resulting in straighter movement

350   (Hedenström & Alerstam, 1995). This can warrant faster forward progress with the same energy

351   expenditure, but only if the thermals drift in the same direction as the primary axis of movement.

352   However, most thermal soaring was convoluted, because stronger winds disrupt thermal lift

353   (Kerlinger, 1989). Where the data exist, our approach could be used to test this hypothesis by

354   including an explicit effect of wind speed.

355   The identification of behavioural states makes it possible to describe time allocation to different

356   movement modes. This can shed light on an animal's decision-making process as it moves

357   through space and adjusts to environmental conditions (Nathan et al., 2008) with flight modes of

358   different efficiencies (Duerr et al., 2012). For example, eagles used different strategies to migrate

359   depending on the season, as reflected in the higher occurrence of orographic flight in autumn and

360   the higher occurrence of gliding and directed thermal soaring in spring. This is intuitive, since

361   the availability of thermals is higher in spring (Duerr et al., 2015).

362   The behavioural models also highlighted differences in flight strategy and performance between

363   age categories. Across both seasons, adults used gliding and directed thermal soaring more than

364   sub-adults, which in turn used more orographic soaring, although these patterns were not

365   reflected in the results for convoluted thermal soaring. Previous studies suggested that, in spring,

366   adults need to move quickly towards the reproductive areas to secure nesting territories, while

367   sub-adults can delay their migration and wait for energetically optimal weather conditions (Duerr

368   et al., 2015; Miller et al., 2016). During spring migration, the relative use of different flight

369 modes also changes as a result of these processes (Katzner et al., 2015). In contrast, our results

370 highlight that, at a broader scale, adults' experience allows them to rely on more efficient flight

371 modes compared to sub-adults overall, despite the constraints of reproduction. This

372 inconsistency with previous work may also be a by-product of the disproportionate classification

373 of behavioural states manually identified as 'unknown' into thermal soaring (Table S4).

374 We also found substantial individual and yearly variability in flight performance, as well as

375 differences in the use of orographic soaring and directed thermal soaring between males and

376 females in autumn (Table S5). The larger size of females and corresponding higher weight might

377 explain some of these patterns, although further investigation is required to explore the

378 underlying functional processes. Because flight modes are characterised by different energetic

379 investment and movement efficiency (Duerr et al., 2012; Hedenstrom, 1993; Hedenström &

380 Alerstam, 1995), their variation among years, seasons, ages, sexes and individuals is relevant for

381 an individual's energy budget, which will ultimately affect its ability to survive and reproduce

382 successfully (Weimerskirch, Louzao, de Grissac, & Delord, 2012). Investigating any spatial or

383 temporal patterns in flight mode distribution could therefore highlight the moments in time or

384 areas that are critical in terms of energy requirements during migration (Shepard et al., 2013).

385 The energetic insight our model can provide also suggests its relevance to the study of other

386 organisms' flight modes and their variation in space and time (Alexander, 2015).

387 Beyond energetics, characterising behavioural states in flying animals is particularly important to

388 evaluate their susceptibility to human activities, informing effective planning and management

389 (Katzner, Brandes, et al., 2012; Péron et al., 2017; Ross-Smith et al., 2016). For example,

390 specific behavioural states, due to their horizontal and vertical characteristics, may put birds at

391 higher risk of collision with turbines (Ross-Smith et al., 2016). For golden eagles in eastern

392 North America, the spatiotemporal distribution of flight modes could be mapped to quantify their

393 overlap with wind power developments within the population's range (Miller et al., 2014) and

394 inform simulation models that estimate collision rates (New, Bjerre, Millsap, Otto, & Runge,

395 2015). In this sense, the mismatch between manual and model classifications may be irrelevant

396 as long as movement features are described correctly, because vulnerability in a state may be

397 more related to average altitude and speed, rather than the type of updraft birds are using.

398 Given that migration patterns are highly affected by weather conditions (Duerr et al., 2015;

399 Lanzone et al., 2012; Miller et al., 2016), the viability of this, and other, populations of long-

400 ranging migratory birds is also threatened by global climate changes (Møller, Rubolini, &

401 Lehikoinen, 2008). The presence of two types of thermal soaring suggests sensitive responses by

402 birds to variation in weather. Thus, major alterations of wind patterns and the increase in

403 frequency of extreme weather events may affect flight decisions and energetic efficiency,

404 potentially compromising birds' migratory abilities (Marra, Francis, Mulvihill, & Moore, 2005).

405 Our model could be used to assess changes in activity budgets following altered weather

406 conditions. In turn, a modified allocation of time to activities with different energetic efficiency

407 could affect the energy balance of these species over the migration and, ultimately, have

408 consequences on their survival and reproductive success (Weimerskirch et al., 2012).

409 From a methodological perspective, the state-space framework presented here advances previous

410 work that modelled altitude data in isolation (Ross-Smith et al., 2016). In addition to altitude, it

411 was the use of ancillary topographical information that supported the identification of orographic

412 soaring, which is associated with ridges and other structures deflecting horizontal winds

413 (Kerlinger, 1989; Mallon, Bildstein, & Katzner, 2016). Selecting appropriate ancillary metrics is

414 critical for the successful discrimination of flight modes that are promoted by specific features of

415 the environment (Murphy et al., 2010). Our analytical approach was unsupervised, in the sense

416 that observed behavioural states were not used to tune the model (Leos-Barajas et al., 2017).

417 However, as part of the preliminary exploration of the tracking dataset, five states were selected

418 and suitable constraints were set to broadly match these states with potential flight modes. The

419 fitting procedure returned posterior estimates of state-specific parameters that were consistent

420 with initial observations and described these putative states in detail.

421 The approach we used aligns with recent analytical efforts to characterise diving and underwater

422 foraging behaviour by marine mammals and seabirds, where depth is used as the third dimension

423 instead of altitude (Bestley et al., 2015; Dean et al., 2013; Isojunno & Miller, 2015; Langrock et

424 al., 2014; Quick et al., 2017). Together with these studies from the marine realm, it therefore

425 represents a step towards developing a fully three-dimensional movement model as data from

426 new sensors (e.g. accelerometry) become available (Leos-Barajas et al., 2017). To this purpose, a

427 semi-Markov extension of the model might be considered (Isojunno & Miller, 2015; Langrock et

428 al., 2014). The distribution of the durations of stays in the various flight modes is unlikely to be

429 geometric, as implied by the Markov property (Langrock et al., 2014), particularly when using a

430 short time step. The posterior predictive checks on our model confirmed that there was residual

431 autocorrelation for some of the response variables under some states (Appendix S5). While this

432 assumption may not affect appropriate behavioural classification, it becomes important when

433 estimated probabilities are used to simulate new tracks.

434

Conclusions

The proliferation of bio-logging devices offers the unique opportunity of detailing individuals'

behavioural patterns at nested scales (Nathan et al., 2008). Identifying different behavioural

modes that arise from animals' response to the underlying habitat and quantifying their

spatiotemporal variation can provide valuable insights into the mechanisms driving behavioural,

energetic and, in the long term, life history decisions (Hays et al., 2016). However, new

statistical tools are required to explore these large datasets and summarise the wide range of

movement features into understandable states (Patterson et al., 2008). Here, we presented a

model that describes a bird's latent behaviour as it switches among flight modes during

migration. Model results highlighted two different patterns of thermal soaring flight. Moreover,

the analysis of the relative occurrence of different flight modes showed yearly, seasonal,

individual, age and sex differences in flight strategy and performance, shedding light on the

functional processes underlying individual behavioural patterns in the context of a dynamic

environment.

21

457 useful discussions on hidden state models. Michael Runge provided valuable comments on an

458 earlier version of this manuscript. Emer Rogan and University College Cork provided desk space

459 to EP. Any use of trade, product, or firm names is for descriptive purposes only and does not

460 imply endorsement by the U.S. Government.

461

462 **Authors' contributions:** All authors contributed to discussions that led to the development of

463 the research project; TM, MB, TK and AD collected and managed eagle telemetry data; EP and

464 LN developed the modelling approach, EP led that exercise and the writing and all authors

465 contributed to revisions.

466

467 **Data accessibility**

468 Data will be made publicly available upon acceptance.

469

470 **References**

471 Alexander, D. E. (2015). *On the wing: insects, pterosaurs, birds, bats and the evolution of*

472   *animal flight*. Oxford University Press, Oxford, UK.

473 Barrios, L., & Rodríguez, A. (2004). Behavioural and environmental correlates of soaring-bird

474   mortality an an-shore wind turbines. *Journal of Applied Ecology*, *41*(1), 72–81.

475   doi:10.1111/j.1365-2664.2004.00876.x

476 Bates, D., Maechler, M., & Bolker, B. (2012). lme4: Linear mixed-effects models using S4

22

477   classes. R package version 0.999999-0. Available at: http://cran.r-

478   project.org/package=lme4.

479   Bestley, S., Jonsen, I., Hindell, M., Harcourt, R. G., & Gales, N. (2015). Taking animal tracking

480   to new depths: synthesizing horizontal–vertical movement relationships for four marine

481   predators. *Ecology*, *96*(2), 417–427. doi:10.1890/14-0469.1

482   Breed, G. a., Costa, D. P., Jonsen, I. D., Robinson, P. W., & Mills-Flemming, J. (2012). State-

483   space methods for more completely capturing behavioral dynamics from animal tracks.

484   *Ecological Modelling*, *235–236*, 49–58. doi:10.1016/j.ecolmodel.2012.03.021

485   Dean, B., Freeman, R., Kirk, H., Leonard, K., Phillips, R. A., Perrins, C. M., & Guilford, T.

486   (2013). Behavioural mapping of a pelagic seabird: combining multiple sensors and a hidden

487   Markov model reveals the distribution of at-sea behaviour. *Journal of the Royal Society*

488   *Interface*, *10*(78), 20120570. doi:10.1098/rsif.2012.0570

489   Dennhardt, A. J., Duerr, A. E., Brandes, D., & Katzner, T. E. (2015). Integrating citizen-science

490   data with movement models to estimate the size of a migratory golden eagle population.

491   *Biological Conservation*, *184*, 68–78. doi:10.1016/j.biocon.2015.01.003

492   Denwood, M. J. (2016). runjags: An R package providing interface utilities, model templates,

493   parallel computing methods and additional distributions for MCMC models in JAGS.

494   *Journal of Statistical Software*, *71*(9), 1–25.

495   Duerr, A. E., Miller, T. A., Lanzone, M., Brandes, D., Cooper, J., O'Malley, K., … Katzner, T.

496   (2012). Testing an emerging paradigm in migration ecology shows surprising differences in

497   efficiency between flight modes. *PLoS ONE*, *7*(4), e35548.

498   doi:10.1371/journal.pone.0035548

499   Duerr, A. E., Miller, T. A., Lanzone, M., Brandes, D., Cooper, J., O'Malley, K., … Katzner, T.

500   (2015). Flight response of slope-soaring birds to seasonal variation in thermal generation.

501   *Functional Ecology*, *29*(6), 779–790. doi:10.1111/1365-2435.12381

502   Evans, J. (2017). spatialEco. R package version 0.0.1-7. <URL: https://CRAN.R-

503   project.org/package=spatialEco>.

504   Gurka, M. J. (2006). Selecting the best linear mixed model under REML. *American Statistician*,

505   *60*(1), 19–26. doi:10.1198/000313006X90396

506   Hays, G. C., Ferreira, L. C., Sequeira, A. M. M., Meekan, M. G., Duarte, C. M., Bailey, H., …

507   Thums, M. (2016). Key questions in marine megafauna movement ecology. *Trends in*

508   *Ecology and Evolution*, *31*(6), 463–475. doi:10.1016/j.tree.2016.02.015

509   Hedenstrom, A. (1993). Migration by soaring or flapping flight in birds: The relative importance

510   of energy cost and speed. *Philosophical Transactions of the Royal Society B: Biological*

511   *Sciences*, *342*(1302), 353–361. doi:10.1098/rstb.1993.0164

512   Hedenström, A., & Alerstam, T. (1995). Optimal flight speed of birds. *Philosophical*

513   *Transactions of the Royal Society B: Biological Sciences*, *348*(1326), 471–487.

514   doi:10.1098/rstb.1995.0082

515   Isojunno, S., & Miller, P. J. O. (2015). Sperm whale response to tag boat presence: biologically

516   informed hidden state models quantify lost feeding opportunities. *Ecosphere*, *6*(1), 1–46.

517   doi:10.1890/ES14-00130.1

518   Jonsen, I., Basson, M., Bestley, S., Bravington, M. V., Patterson, T. A., Pedersen, M. W., …

24

519   Wotherspoon, S. J. (2013). State-space models for bio-loggers: A methodological road map.

520   *Deep Sea Research Part II: Topical Studies in Oceanography*, *88–89*, 34–46.

521   doi:10.1016/j.dsr2.2012.07.008

522 Katzner, T. E., Brandes, D., Miller, T., Lanzone, M., Maisonneuve, C., Tremblay, J. A., …

523   Merovich, G. T. (2012). Topography drives migratory flight altitude of golden eagles:

524   Implications for on-shore wind energy development. *Journal of Applied Ecology*, *49*(5),

525   1178–1186. doi:10.1111/j.1365-2664.2012.02185.x

526 Katzner, T. E., Smith, B. W., Miller, T. A., Brandes, D., Cooper, J., Brauning, D., … Bildstein,

527   K. L. (2012). Status, biology, and conservation priorities for North America's eastern

528   Golden Eagle (*Aquila chrysaetos*) population. *The Auk*, *129*, 168–176.

529 Katzner, T. E., Turk, P. J., Duerr, A. E., Miller, T. A., Lanzone, M. J., Cooper, J. L., …

530   Lemaître, J. (2015). Use of multiple modes of flight subsidy by a soaring terrestrial bird, the

531   golden eagle *Aquila chrysaetos*, when on migration. *Journal of the Royal Society Interface*,

532   *12*, 20150530. doi:10.1098/rsif.2015.0530

533 Kays, R., Crofoot, M. C., Jetz, W., & Wikelski, M. (2015). Terrestrial animal tracking as an eye

534   on life and planet. *Science*, *348*(6240), 1222–1232. doi:10.1126/science.aaa2478

535 Kerlinger, P. (1989). *Flight strategies of migrating hawks*. University of Chicago Press, Chicago.

536 Klaassen, R. H. G., Strandberg, R., Hake, M., & Alerstam, T. (2008). Flexibility in daily travel

537   routines causes regional variation in bird migration speed. *Behavioral Ecology and*

538   *Sociobiology*, *62*(9), 1427–1432. doi:10.1007/s00265-008-0572-x

539 Langrock, R., King, R., Matthiopoulos, J., Thomas, L., Fortin, D., & Morales, J. M. (2012).

540   Flexible and practical modeling of animal telemetry data: hidden Markov models and

541   extensions. *Ecology*, *93*(11), 2336–2342. doi:10.1371/journal.pbio.1000178

542 Langrock, R., Marques, T. A., Baird, R. W., & Thomas, L. (2014). Modeling the diving behavior

543   of whales: A latent-variable approach with feedback and semi-Markovian components.

544   *Journal of Agricultural, Biological, and Environmental Statistics*, *19*(1), 82–100.

545   doi:10.1007/s13253-013-0158-6

546 Lanzone, M. J., Miller, T. A., Turk, P., Brandes, D., Halverson, C., Maisonneuve, C., …

547   Katzner, T. (2012). Flight responses by a migratory soaring raptor to changing

548   meteorological conditions. *Biology Letters*, *8*(5), 710–713. doi:10.1098/rsbl.2012.0359

549 Leos-Barajas, V., Photopoulou, T., Langrock, R., Patterson, T. A., Watanabe, Y. Y., Murgatroyd,

550   M., & Papastamatiou, Y. P. (2017). Analysis of animal accelerometer data using hidden

551   Markov models. *Methods in Ecology and Evolution*, *8*, 161–173. doi:10.1111/2041-

552   210X.12657

553 Lunn, D., Jackson, C., Best, N., Thomas, A., & Spiegelhalter, D. (2013). *The BUGS book: A*

554   *practical introduction to Bayesian analysis*. Boca Raton, Florida, USA: Chapman &

555   Hall/CRC.

556 Mallon, J. M., Bildstein, K. L., & Katzner, T. E. (2016). In-flight turbulence benefits soaring

557   birds. *Auk*, *133*(1), 79–85. doi:10.1642/AUK-15-114.1

558 Marra, P. P., Francis, C. M., Mulvihill, R. S., & Moore, F. R. (2005). The influence of climate on

559   the timing and rate of spring bird migration. *Oecologia*, *142*(2), 307–315.

560   doi:10.1007/s00442-004-1725-x

561   McClintock, B. T., King, R., Thomas, L., Matthiopoulos, J., McConnell, B. J., & Morales, J. M.

562   (2012). A general discrete-time modeling framework for animal movement using multistate

563   random walks. *Ecological Monographs*, *82*(3), 335–349. doi:10.1890/11-0326.1

564   McClintock, B. T., London, J. M., Cameron, M. F., & Boveng, P. L. (2017). Bridging the gaps in

565   animal movement: Hidden behaviors and ecological relationships revealed by integrated

566   data streams. *Ecosphere*, *8*(3). doi:10.1002/ecs2.1751

567   McClintock, B. T., Russell, D. J. F., Matthiopoulos, J., & King, R. (2013). Combining individual

568   animal movement and ancillary biotelemetry data to investigate population-level activity

569   budgets. *Ecology*, *94*(4), 838–849.

570   Michelot, T., Langrock, R., Bestley, S., Jonsen, I. D., Photopoulou, T., & Patterson, T. A.

571   (2017). Estimation and simulation of foraging trips in land-based marine predators.

572   *Ecology*, *98*(7), 1932–1944. doi:10.1002/ecy.1880

573   Miller, T. A., Brooks, R. P., Lanzone, M., Brandes, D., Cooper, J., O'Malley, K., … Katzner, T.

574   (2014). Assessing risk to birds from industrial wind energy development via paired resource

575   selection models. *Conservation Biology*, *28*(3), 745–755. doi:10.1111/cobi.12227

576   Miller, T. A., Brooks, R. P., Lanzone, M. J., Brandes, D., Cooper, J., Tremblay, J. A., …

577   Katzner, T. E. (2016). Limitations and mechanisms influencing the migratory performance

578   of soaring birds. *Ibis*, *158*, 116–134. doi:10.1111/ibi.12331

579   Møller, A. P., Rubolini, D., & Lehikoinen, E. (2008). Populations of migratory bird species that

580   did not show a phenological response to climate change are declining. *Proceedings of the*

581   *National Academy of Sciences of the United States of America*, *105*(42), 16195–16200.

582   doi:10.1073/pnas.0803825105

583   Morales, J. M., Haydon, D. T., Frair, J., Holsinger, K. E., & Fryxell, J. M. (2004). Extracting

584   more out of relocation data: building movement models as mixtures of random walks.

585   *Ecology*, *85*(9), 2436–2445. doi:10.1890/03-0269

586   Murphy, M. A., Evans, J. S., & Storfer, A. (2010). Quantifying Bufo boreas connectivity in

587   Yellowstone National Park with landscape genetics. *Ecology*, *91*(1), 252–61.

588   doi:10.1890/08-0879.1

589   Nathan, R., Getz, W. M., Revilla, E., Holyoak, M., Kadmon, R., Saltz, D., & Smouse, P. E.

590   (2008). A movement ecology paradigm for unifying organismal movement research.

591   *Proceedings of the National Academy of Sciences*, *105*(49), 19052–19059.

592   doi:10.1073/pnas.0800375105

593   New, L., Bjerre, E., Millsap, B., Otto, M. C., & Runge, M. C. (2015). A collision risk model to

594   predict avian fatalities at wind facilities: An example using golden eagles, *Aquila*

595   *chrysaetos*. *PLoS ONE*, *10*(7), 1–12. doi:10.1371/journal.pone.0130978

596   Patterson, T. A., Thomas, L., Wilcox, C., Ovaskainen, O., & Matthiopoulos, J. (2008). State-

597   space models of individual animal movement. *Trends in Ecology & Evolution*, *23*(2), 87–

598   94. doi:10.1016/j.tree.2007.10.009

599   Péron, G., Fleming, C. H., Duriez, O., Fluhr, J., Itty, C., Lambertucci, S., … Calabrese, J. M.

600   (2017). The energy landscape predicts flight height and wind turbine collision hazard in

601   three species of large soaring raptor. *Journal of Applied Ecology*, *54*(6), 1895–1906.

602   doi:10.1111/1365-2664.12909

603   Pirotta, E., Edwards, E. W. J., New, L., & Thompson, P. M. (2018). Central place foragers and

604   moving stimuli: a hidden-state model to discriminate the processes affecting movement.

605   *Journal of Animal Ecology*, *In press*. doi:10.1111/1365-2656.12830

606   Plummer, M., Best, N., Cowles, K., & Vines, K. (2006). CODA: Convergence Diagnosis and

607   Output Analysis for MCMC. *R News*, *6*, 7–11.

608   Poessel, S. A., Duerr, A. E., Hall, J. C., Braham, M. A., & Katzner, T. E. (2018). Improving

609   estimation of flight altitude in wildlife telemetry studies. *Journal of Applied Ecology*, 1–7.

610   doi:10.1111/1365-2664.13135

611   Quick, N. J., Isojunno, S., Sadykova, D., Bowers, M., Nowacek, D. P., & Read, A. J. (2017).

612   Hidden Markov models reveal complexity in the diving behaviour of short-finned pilot

613   whales. *Scientific Reports*, *7*, 45765. doi:10.1038/srep45765

614   R Development Core Team. (2016). R: A language and environment for statistical computing. R

615   Foundation for Statistical Computing, Vienna, Austria. ISBN 3-900051-07-0, URL

616   http://www.R-project.org/.

617   Ross-Smith, V. H., Thaxter, C. B., Masden, E. A., Shamoun-Baranes, J., Burton, N. H. K.,

618   Wright, L. J., … Thompson, D. (2016). Modelling flight heights of lesser black-backed

619   gulls and great skuas from GPS: a Bayesian approach. *Journal of Applied Ecology*, *53*(6),

620   1676–1685. doi:10.1111/1365-2664.12760

621   Shepard, E. L. C., Wilson, R. P., Rees, W. G., Grundy, E., Lambertucci, S. A., & Vosper, S. B.

622   (2013). Energy landscapes shape animal movement ecology. *The American Naturalist*,

623   *182*(3), 298–312. doi:10.1086/671257

624   Stephens, M. (2000). Dealing with label switching in mixture models. *Journal of the Royal*

625   *Statistical Society: Series B (Statistical Methodology)*, *62*(4), 795–809.

626   Weimerskirch, H., Louzao, M., de Grissac, S., & Delord, K. (2012). Changes in wind pattern

627   alter albatross distribution and life-history traits. *Science*, *335*, 211–214.

628   doi:10.1126/science.1210270

629   Williams, H. J., Shepard, E. L. C., Duriez, O., & Lambertucci, S. A. (2015). Can accelerometry

630   be used to distinguish between flight types in soaring birds? *Animal Biotelemetry*, *3*(1), 45.

631   doi:10.1186/s40317-015-0077-0

632

633   **Supporting Information**

634   Additional supporting information may be found in the online version of this article.

635   **Table S1.** Number of tracks available per individual in each year.

636   **Table S2.** Description of variables and model parameters.

637   **Appendix S1.** Details of prior distributions.

638   **Appendix S2.** JAGS code for the model.

639   **Table S3.** Posterior estimates of model parameters.

640   **Figure S1.** State-dependent emission distributions of the four response variables.

641   **Figure S2.** Example of time series of true altitudes from a track segment.

642   **Table S4.** Confusion matrix comparing manual and model state classifications.

643   **Table S5.** Results of model selection for the behavioural models.

644   **Figure S3.** Dot plots of the random effects of individual and year.

645   **Appendix S3.** Reformulation of the model allowing for missing data.

646   **Appendix S4.** Analysis of simulated data.

647   **Appendix S5.** Posterior predictive checks.

648   **Figure S4**. Results of the posterior predictive checks.

649   **Figure S5.** Autocorrelation function (ACF) plots for the response variables by state in the

650   original and simulated data.
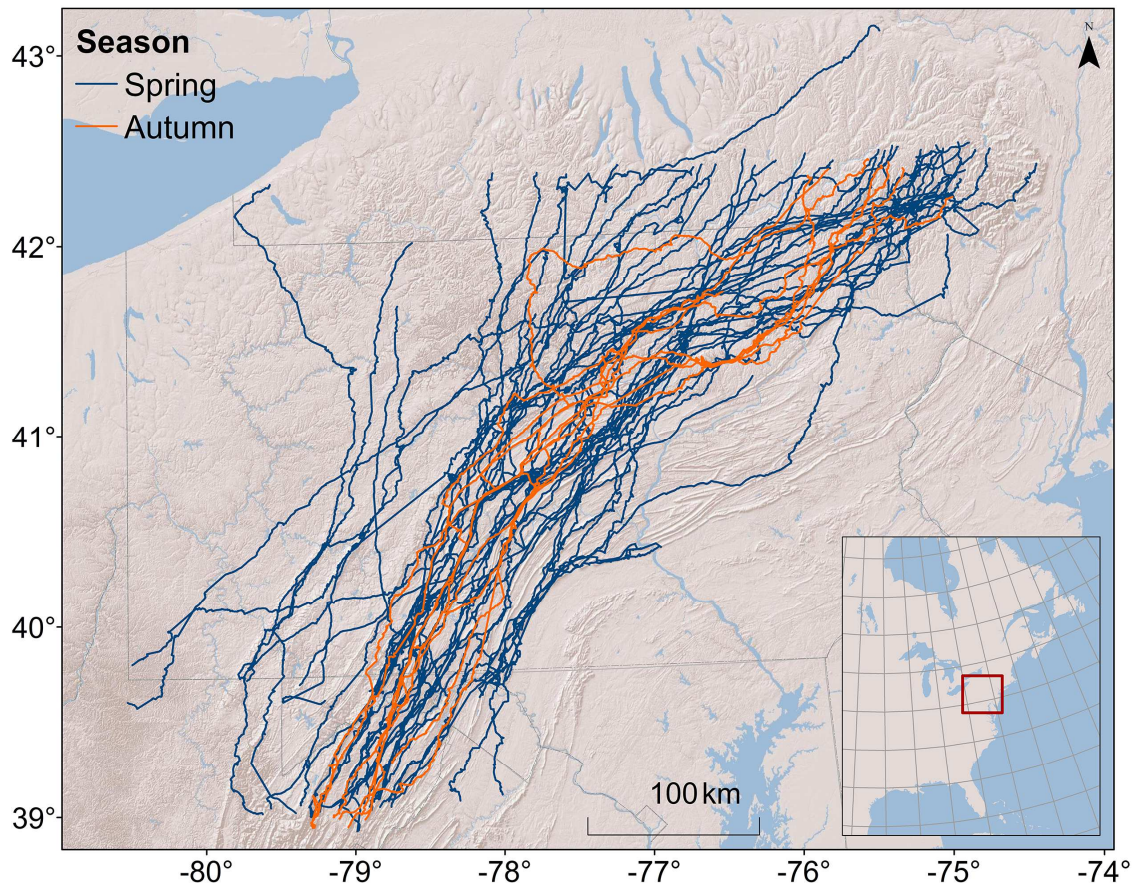
651 **Tables**

652

653 Table 1. Estimated golden eagle activity budget, across both migration seasons and by migration

654 season.

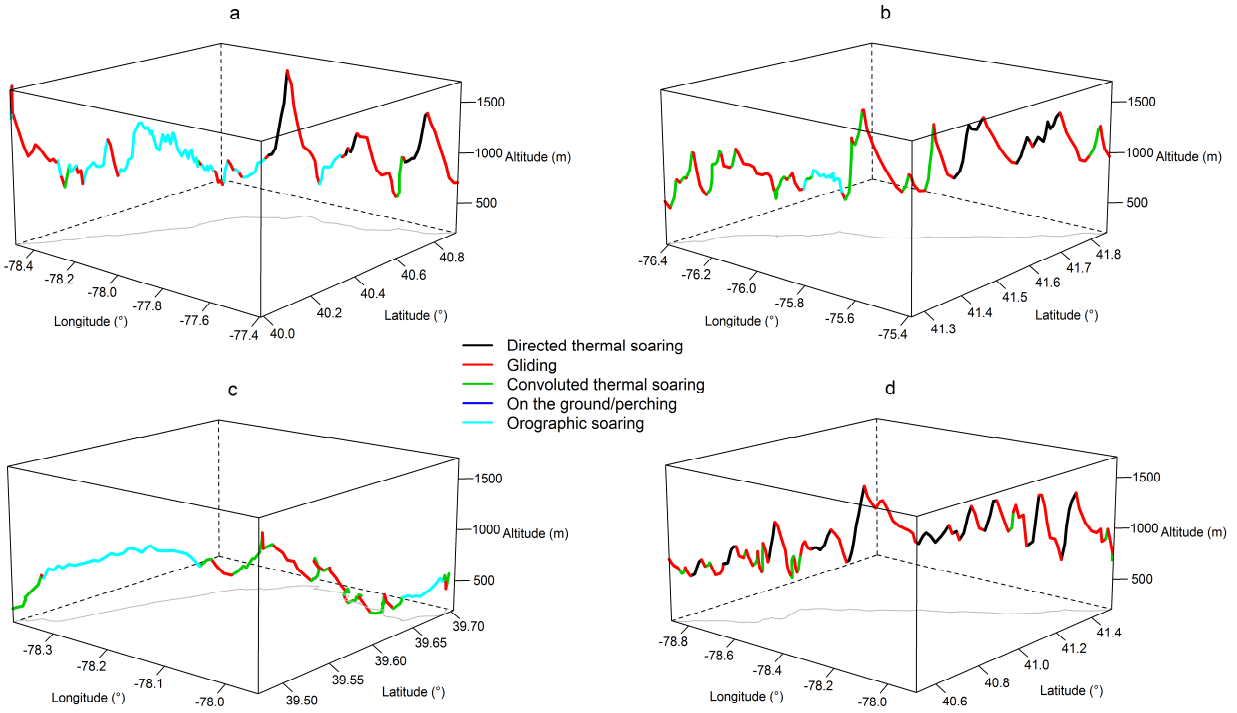|	*Directed thermal soaring*	*Gliding*	*Convoluted thermal soaring*	*On the ground or perching*	*Orographic soaring*
Overall	2%	31%	38%	9%	20%
Spring	3%	32%	37%	10%	18%
Autumn	0%	24%	43%	8%	25%

655

Figures

659   Figure 1. Map of study area and golden eagle tracks in autumn (48 tracks) and in spring (10

660   tracks).

661

Figure 2. Segments of three-dimensional golden eagle tracks. Tracks are coloured based on
model posterior medians of the behavioural state at each minute *t*. In grey, the shadow of the
track projected onto the horizontal plane. The posterior median of true altitudes is used for the
vertical dimension.
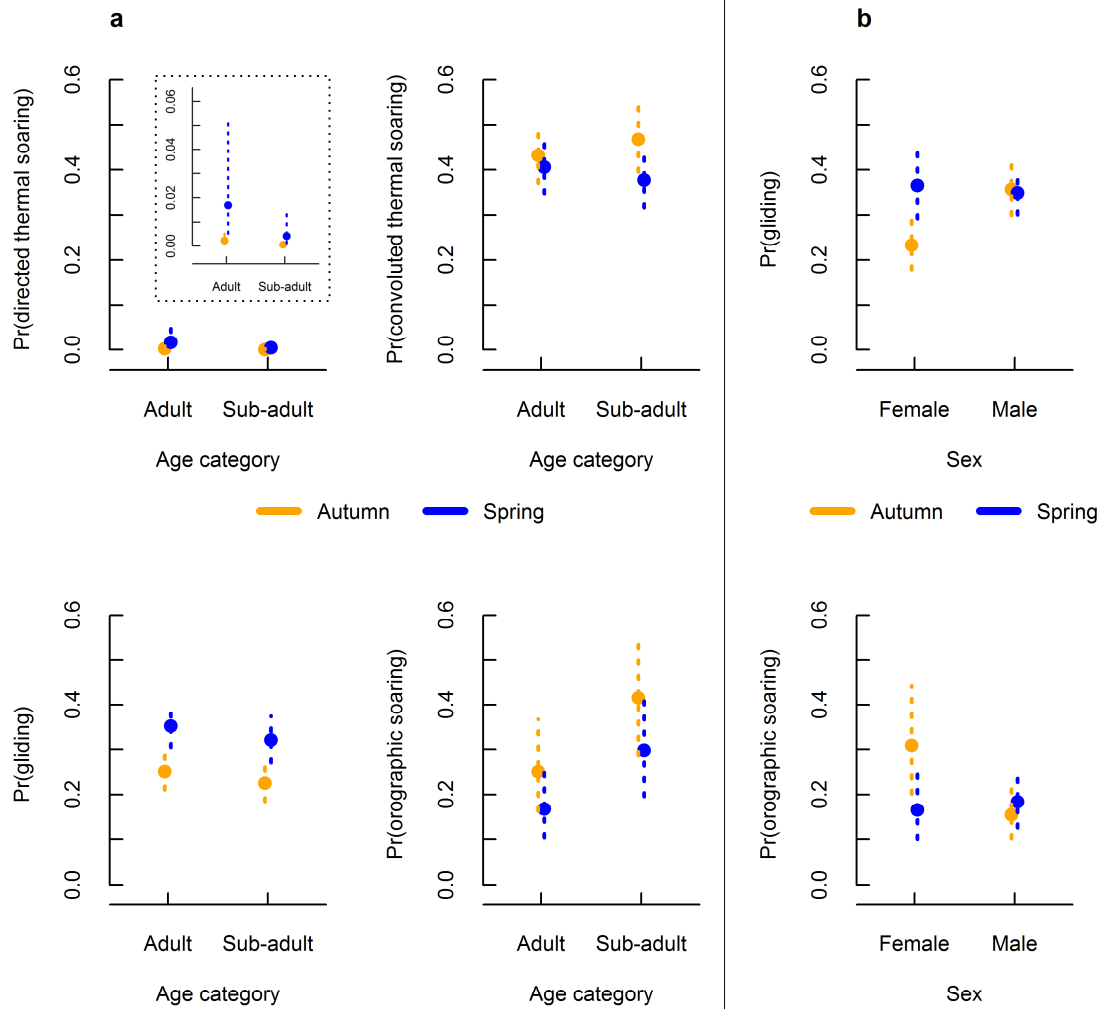
Figure 3. Results of the behavioural models by state (mean and 95% confidence intervals). The y-axis was standardised across plots, but the top left plot also includes a zoomed inset graph (dotted box) for clarity. a) Effect of season and age category on the proportional occurrence of each state. b) Effect of season and sex on the proportional occurrence of gliding and orographic soaring. Results for the two forms of thermal soaring are not reported because the effect of sex was not retained by model selection.

Supporting information

Table S1. Number of tracks available per individual in each year.

Individual ID	Year							
	2009	*2010*	*2011*	*2012*	*2013*	*2014*	*2015*	*2016*
95	0	0	2	1	0	0	0	0
301	0	1	0	0	0	0	0	0
376	0	1	0	0	0	0	0	0
434	0	0	1	0	0	0	0	0
483	0	0	1	0	0	0	0	0
558	0	0	1	0	0	0	0	0
749	0	0	1	0	0	0	0	0
2851	0	1	0	0	0	0	0	0
3206	0	0	1	0	0	0	0	0
3546	0	0	1	0	0	0	0	0
3553	0	1	0	0	0	0	0	0
3785	0	0	0	2	2	2	0	0
4189	0	0	0	1	0	0	0	0
4195	0	0	0	1	1	0	0	0
4379	0	0	0	2	1	2	1	1
4533	1	0	0	0	0	0	0	0
4733	0	1	1	1	1	1	1	0
4782	0	1	1	0	0	0	0	0
5061	0	0	0	0	1	0	0	0
5244	0	0	0	1	1	0	0	0
5269	0	0	0	2	2	1	0	0
6960	1	0	0	0	0	0	0	0
7231	0	0	0	2	1	1	0	0
7454	0	0	0	1	0	0	0	0
7878	0	0	2	1	0	0	0	0
8107	1	0	0	0	0	0	0	0
9013	0	0	0	1	0	0	0	0
9287	0	0	0	0	0	1	0	0

Table S2. Description of variables and model parameters. The subscript *t* indicates a time-dependent variable, while the subscript *i* indicates a state-dependent parameter. HSP stands for hierarchical slope position.

Class	Symbol	Name	Definition
Data	x_t	Step length	Distance between consecutive locations
	θ_t	Turning angle	Angle between consecutive steps
	a_t	Altitude (observed)	Altitude above sea level as measured by the GPS
	h_t	Hierarchical slope position	Measure of topographic exposure (Murphy, Evans, & Storfer, 2010)
	$\mathbf{y_t}$	Data vector	Vector of observations of the three movement metrics (*x*, *θ*, *a* and *h*)
Underlying variables	s_t	State	Latent behavioural state
	v_t	Altitude (true)	True altitude above sea level
Model parameters	π_i	Vertical drift	Mean change in altitude under state *i*
	σ_i	Altitude standard deviation	State-specific variation around altitude change
	ε	Altitude observation error	Altitude uncertainty due to GPS measurement error
	ρ_i	Concentration	State-dependent variability in turning angles
	α_i	Scale	Scale parameter for the state-dependent distribution of step lengths
	β_i	Shape	Shape parameter for the state-dependent distribution of step lengths
	κ_i	Mean HSP	State-dependent mean of hierarchical slope position
	ω_i	Standard deviation HSP	State-dependent standard deviation of hierarchical slope position
	$\gamma_{i,j}$	Transition probability	Probability of switching between state *i* and state *j*
	φ_i	Initial state probability	Probability of being in state *i* at the start of a track

Appendix S1. Details of prior distributions.

Priors for state 1 (directed thermal soaring): The vertical drift had a truncated positive prior, so that under this state the bird was assumed to be gaining altitude. The variability in vertical drift was constrained between 0 and 150 m. Turning angles were assumed to be relatively more directed (i.e. concentration > 0.5) than in other states. Priors for parameters α and β were defined on a logarithmic scale to avoid meaningless negative values. The mean and standard deviation of hierarchical slope position was unconstrained.

Priors for state 2 (gliding): The vertical drift had the same absolute value and variability as in state 1, but opposite sign, i.e. the bird was decreasing its altitude. The distribution of turning angles was assumed to be the same as in state 1. This state had the same step length distribution as state 1. The mean and standard deviation of hierarchical slope position was the same as in state 1. We also investigated a model where the descending state (state 2) had the same horizontal features of state 3, but this model did not converge, suggesting that, while ascending behaviour can be either horizontally straight or convoluted, descending behaviour tends to be predominantly straight, as expected from gliding flight (Katzner et al., 2015).

Priors for state 3 (convoluted thermal soaring): The prior for vertical drift was truncated to represent altitude gain. The variability in vertical drift was constrained between 0 and 150 m. This state was constrained to be at most as directed as states 1, 2 and 5. Steps were constrained to be smaller than under state 1 and 2. The mean and standard deviation of hierarchical slope position was the same as in state 1 and 2.

Priors for state 4 (on the ground or perching): The bird was assumed to remain at a stable altitude, on average (i.e. mean vertical drift was set to 0, with a standard deviation fixed at 10 m

to represent small changes in altitude due to terrain features). Horizontal movement was assumed to be relatively more convoluted (i.e. concentration < 0.5). Steps were constrained to be smaller than under state 3.

Priors for state 5 (orographic soaring): The bird was assumed to remain at a stable altitude, on average (i.e. mean vertical drift was set to 0). The variability in vertical drift was constrained between 0 and 150 m. The distribution of turning angles was assumed to be the same as in state 1. Steps were constrained to be smaller than under state 1 and 2. Hierarchical slope position has higher values along ridges and was thus assumed to have mean higher in this state than in state 1, 2 and 3, while its variability was unconstrained.

States at time t were not previously labelled, and the model assigned a state to each time step based on the posterior estimates of the parameters. We used an unbiased and relatively uninformative Dirichlet(1,1,1,1,1) prior for the transition probabilities $\gamma_{i,1\ldots5}$ from each state i to all states, as well as for the probabilities of being in each state at the beginning of a track or track segment $\varphi_{1,\ldots,5}$. The standard deviation of the observation model for altitude (ε) was set to 25 m. While it would be preferable to estimate this parameter directly from the data, such standard deviation was found to be confounded with the standard deviation of true altitude. However, the fixed value we used was larger than the reported accuracy of the GPS devices (± 15 m; Lanzone et al., 2012), as a conservative way to account for error variation due to fix quality and other factors (Péron et al., 2017).

Description	Parameter	Prior
Vertical drift (altitude)	π_1	*Truncated Normal* (100, 45) [30,]
	π_2	- π_1
	π_3	*Truncated Normal* (40, 45) [30,]
	π_4	0
	π_5	0
Standard deviation (altitude)	σ_1	*Uniform* (0, 150)
	σ_2	σ_1
	σ_3	*Uniform* (0, 150)
	σ_4	10
	σ_5	*Uniform* (0, 150)
Concentration (turning angle)	ρ_1	*Uniform* (0.5, 1)
	ρ_2	ρ_1
	ρ_3	*Uniform* (0, ρ_1)
	ρ_4	*Uniform* (0, 0.5)
	ρ_5	ρ_1
Scale (step length)	$\log(\alpha_1)$	*Uniform* (-1, 7)
	$\log(\alpha_2)$	$\log(\alpha_1)$
	$\log(\alpha_3)$	*Uniform* (-1, $\log(\alpha_1)$)
	$\log(\alpha_4)$	*Uniform* (-1, $\log(\alpha_3)$)
	$\log(\alpha_5)$	*Uniform* (-1, $\log(\alpha_1)$)
Shape (step length)	$\log(\beta_1)$	*Uniform* (-1, 2)
	$\log(\beta_2)$	$\log(\beta_1)$
	$\log(\beta_3)$	*Uniform* (-1, 2)
	$\log(\beta_4)$	*Uniform* (-1, 2)
	$\log(\beta_5)$	*Uniform* (-1, 2)
Mean (hierarchical slope position)	κ_1	*Normal* (0.3, 0.3)
	κ_2	κ_1
	κ_3	κ_1
	κ_4	*Normal* (0.3, 0.3)
	κ_5	*Truncated Normal* (0.4, 0.3) [κ_1,]
Standard deviation (hierarchical slope position)	ω_1	*Uniform* (0, 0.2)
	ω_2	ω_1
	ω_3	ω_1
	ω_4	*Uniform* (0, 0.2)
	ω_5	*Uniform* (0, 0.2)
Transition probabilities from each state i	$\gamma_{i,1\ldots5}$	*Dirichlet* (1,1,1,1,1)
Initial state probabilities	$\varphi_{1\ldots5}$	*Dirichlet* (1,1,1,1,1)

Appendix S2. JAGS code for the model.

```
model
{

##Priors and constraints by state##

#Mean vertical drift
pi[1] ~ dnorm(100,0.0005)T(30,)
pi[2] <- -pi[1]
pi[3] ~ dnorm(40,0.0005)T(30,)
pi[4] <- 0
pi[5] <- 0

#STD vertical drift
sigma[1] ~ dunif(0,150)
sigma[2] <- sigma[1]
sigma[3] ~ dunif(0,150)
sigma[4] <- 10
sigma[5] ~ dunif(0,150)
for (i in 1:nstates){
 upsi.tau[i] <- 1/sigma[i]/sigma[i] #transform STD to precision
 }

#Concentration parameter for turning angle
rho[1] ~ dunif(0.5,1)
rho[2] <- rho[1]
rho[3] ~ dunif(0,rho[1])
rho[4]  ~ dunif(0,0.5)
```

```
rho[5] <- rho[1]

#Mean turning angle (fixed)
mu <- 0

#Parameters for step length distribution (on log scale)
logalpha[1] ~ dunif(-1,log.maxalpha)
logalpha[2] <- logalpha[1]
logalpha[3] ~ dunif(-1,logalpha[1])
logalpha[4] ~ dunif(-1,logalpha[3])
logalpha[5] ~ dunif(-1,logalpha[1])


logbeta[1] ~ dunif(-1,log.maxbeta)
logbeta[2] <- logbeta[1]
logbeta[3] ~ dunif(-1,log.maxbeta)
logbeta[4] ~ dunif(-1,log.maxbeta)
logbeta[5] ~ dunif(-1,log.maxbeta)


for (i in 1:nstates){
 alpha[i] <- exp(logalpha[i])
 beta[i] <- exp(logbeta[i])
 #JAGS uses different Weibull parameterization than R
 lambda[i] <- 1/pow(alpha[i],beta[i])
 }

#Mean HSP
kappa[1] ~ dnorm(0.3,10)
kappa[2] <- kappa[1]
kappa[3] <- kappa[1]
kappa[4] ~ dnorm(0.3,10)
```

```
kappa[5] ~ dnorm(0.4,10)T(kappa[1],)

#STD HSP
omega[1] ~ dunif(0,0.2)
omega[2] <- omega[1]
omega[3] <- omega[1]
omega[4] ~ dunif(0,0.2)
omega[5] ~ dunif(0,0.2)
for (i in 1:nstates){
 hsp.tau[i] <- 1/omega[i]/omega[i] #transform STD to precision
 }

#Initial state probabilities
phi[1:nstates] ~ ddirch(phiprior[1:nstates])

#Transition probabilities
for (i in 1:nstates){
 gamma[i,1:nstates] ~ ddirch(phiprior[1:nstates])
 }

#Observation error on altitude
epsilon <- 25
a.tau <- 1/epsilon/epsilon

##Model##
for (k in 1:ntracks){                              #loop over track segments
 s[Xidx[k]] ~ dcat(phi[1:nstates])                 #initial behavioural state
 upsilon[Xidx[k]+1] ~ dnorm(a[Xidx[k]+1], a.tau)      #initial true altitude

 #State proportions
```

```
state.cnt[1,Xidx[k]] <- equals(s[Xidx[k]],1)
state.cnt[2,Xidx[k]] <- equals(s[Xidx[k]],2)
state.cnt[3,Xidx[k]] <- equals(s[Xidx[k]],3)
state.cnt[4,Xidx[k]] <- equals(s[Xidx[k]],4)
state.cnt[5,Xidx[k]] <- equals(s[Xidx[k]],5)

for (t in (Xidx[k]+1):(Xidx[k+1]-2)){                    #loop over time steps
  s[t] ~ dcat(gamma[s[t-1],1:nstates])                   #behavioural state

  upsi.mean[t+1] <- upsilon[t] + pi[s[t]]                #mean altitude
  upsilon[t+1] ~ dnorm(upsi.mean[t+1], upsi.tau[s[t]])   #process error (true altitude)
  a[t+1] ~ dnorm(upsilon[t+1], a.tau)                    #observed altitude (with
   observation error)

  h[t] ~ dnorm(kappa[b[t]], hsp.tau[b[t]])               #Hierarchical Slope Position

  x[t] ~ dweib(beta[s[t]],lambda[s[t]])                  #step length

  #"ones" trick to sample from the Wrapped Cauchy distribution
  ones[t] ~ dbern(wC[t])
  wC[t] <- ( 1/(2*Pi)*(1-rho[s[t]]*rho[s[t]])/(1+rho[s[t]]*rho[s[t]]-
  2*rho[s[t]]*cos(theta[t]-mu)) )/500

  #State proportions
  state.cnt[1,t] <- equals(s[t],1)
  state.cnt[2,t] <- equals(s[t],2)
  state.cnt[3,t] <- equals(s[t],3)
  state.cnt[4,t] <- equals(s[t],4)
  state.cnt[5,t] <- equals(s[t],5)
```

```
  }#close temporal loop

 state.cnt[1,Xidx[k+1]-1]<-0
 state.cnt[2,Xidx[k+1]-1]<-0
 state.cnt[3,Xidx[k+1]-1]<-0
 state.cnt[4,Xidx[k+1]-1]<-0
 state.cnt[5,Xidx[k+1]-1]<-0

 }#close track loop

#Monitor state convergence
delta[1] <- sum(state.cnt[1,1:(Xidx[ntracks+1]-1)])/(Xidx[ntracks+1]-1-ntracks)
delta[2] <- sum(state.cnt[2,1:(Xidx[ntracks+1]-1)])/(Xidx[ntracks+1]-1-ntracks)
delta[3] <- sum(state.cnt[3,1:(Xidx[ntracks+1]-1)])/(Xidx[ntracks+1]-1-ntracks)
delta[4] <- sum(state.cnt[4,1:(Xidx[ntracks+1]-1)])/(Xidx[ntracks+1]-1-ntracks)
delta[5] <- sum(state.cnt[5,1:(Xidx[ntracks+1]-1)])/(Xidx[ntracks+1]-1-ntracks)

}
```

Table S3. Posterior estimates of model parameters (median and 95% highest posterior density interval). For each parameter, the table also reports the effective sample size and convergence diagnostics: upper confidence interval (CI) of the Brooks-Gelman-Rubin (BGR) diagnostic and percentage of Monte Carlo error (MCE) to sample standard deviation (SSD).

Description	Parameter	Lower (2.5%)	Median	Upper (97.5%)	Effective sample size	BGR diagnostic (upper CI)	% MCE/SSD
Vertical drift (altitude)	$\pi_1 = -\pi_2$	74	76	77	3315	1.01	1.74
	π_3	52	53	55	3509	1	1.69
Standard deviation (altitude)	$\sigma_1 = \sigma_2$	64	65	66	2527	1	2.10
	σ_3	71	72	74	2652	1	1.95
	σ_5	95	97	99	2621	1.01	1.96
Concentration (turning angle)	$\rho_1 = \rho_2 = \rho_5$	0.83	0.84	0.84	3874	1.01	1.63
	ρ_3	0.62	0.63	0.64	3552	1.01	1.69
	ρ_4	0.00	0.00	0.00	4286	1	1.53
Scale (step length)	$\alpha_1 = \alpha_2$	1058	1065	1071	1515	1	2.59
	α_3	385	390	395	1437	1	2.69
	α_4	22	23	24	1454	1.02	2.62
	α_5	654	663	672	2346	1	2.09
Shape (step length)	$\beta_1 = \beta_2$	3.56	3.61	3.67	2360	1	2.07
	β_3	1.87	1.90	1.92	3568	1.01	1.75
	β_4	0.90	0.93	0.96	1155	1.02	3.22
	β_5	1.80	1.83	1.87	2860	1	1.88
Mean	$\kappa_1 = \kappa_2 = \kappa_3$	0.326	0.327	0.328	942	1.03	3.29
	κ_4	0.375	0.378	0.380	3931	1.01	1.68

(hierarchical slope position)	κ_5	0.448	0.450	0.452	901	1.01	3.39
Standard deviation (hierarchical slope position)	$\omega_1 = \omega_2 = \omega_3$	0.049	0.050	0.050	1663	1.02	2.49
	ω_4	0.070	0.071	0.073	4045	1	1.58
	ω_5	0.052	0.053	0.054	3158	1.01	1.80
State proportions	δ_1	0.02	0.03	0.03	504	1.01	4.45
	δ_2	0.30	0.31	0.31	1421	1	2.74
	δ_3	0.37	0.37	0.38	691	1.03	3.82
	δ_4	0.09	0.09	0.10	523	1.05	4.47
	δ_5	0.20	0.20	0.21	430	1.05	4.86
Transition probabilities	$\gamma_{1,1}$	0.754	0.785	0.815	2785	1	1.90
	$\gamma_{2,1}$	0.012	0.015	0.018	1481	1.01	2.68
	$\gamma_{3,1}$	0.001	0.002	0.003	1650	1	2.64
	$\gamma_{4,1}$	0.000	0.000	0.001	4657	1	1.47
	$\gamma_{5,1}$	0.000	0.000	0.001	2867	1	1.89
	$\gamma_{1,2}$	0.169	0.199	0.229	2414	1	2.08
	$\gamma_{2,2}$	0.714	0.723	0.732	4500	1	1.49
	$\gamma_{3,2}$	0.172	0.179	0.186	4091	1	1.56
	$\gamma_{4,2}$	0.000	0.000	0.001	4500	1.01	1.49
	$\gamma_{5,2}$	0.058	0.064	0.070	3831	1	1.62
	$\gamma_{1,3}$	0.000	0.001	0.006	3571	1	1.67
	$\gamma_{2,3}$	0.214	0.223	0.231	4223	1	1.54
	$\gamma_{3,3}$	0.781	0.789	0.796	4153	1	1.55
	$\gamma_{4,3}$	0.029	0.035	0.042	3100	1.01	1.79
	$\gamma_{5,3}$	0.020	0.025	0.029	2982	1	1.84
	$\gamma_{1,4}$	0.000	0.001	0.003	4644	1.01	1.47
	$\gamma_{2,4}$	0.000	0.001	0.002	3772	1	1.64
	$\gamma_{3,4}$	0.010	0.012	0.014	3936	1.01	1.61
	$\gamma_{4,4}$	0.938	0.946	0.953	3647	1.02	1.65

	$\gamma_{5,4}$	0.016	0.019	0.022	3559	1	1.68
	$\gamma_{1,5}$	0.005	0.013	0.026	1897	1	2.37
	$\gamma_{2,5}$	0.034	0.038	0.042	2987	1.01	1.86
	$\gamma_{3,5}$	0.016	0.019	0.022	2668	1	1.98
	$\gamma_{4,5}$	0.014	0.018	0.024	2828	1.01	1.88
	$\gamma_{5,5}$	0.884	0.892	0.899	3598	1	1.67
Initial state probabilities	φ_1	0.005	0.019	0.041	1686	1	2.46
	φ_2	0.092	0.155	0.221	2946	1	1.85
	φ_3	0.378	0.447	0.514	3456	1.01	1.70
	φ_4	0.109	0.137	0.169	4029	1.01	1.58
	φ_5	0.198	0.238	0.286	3053	1.01	1.83
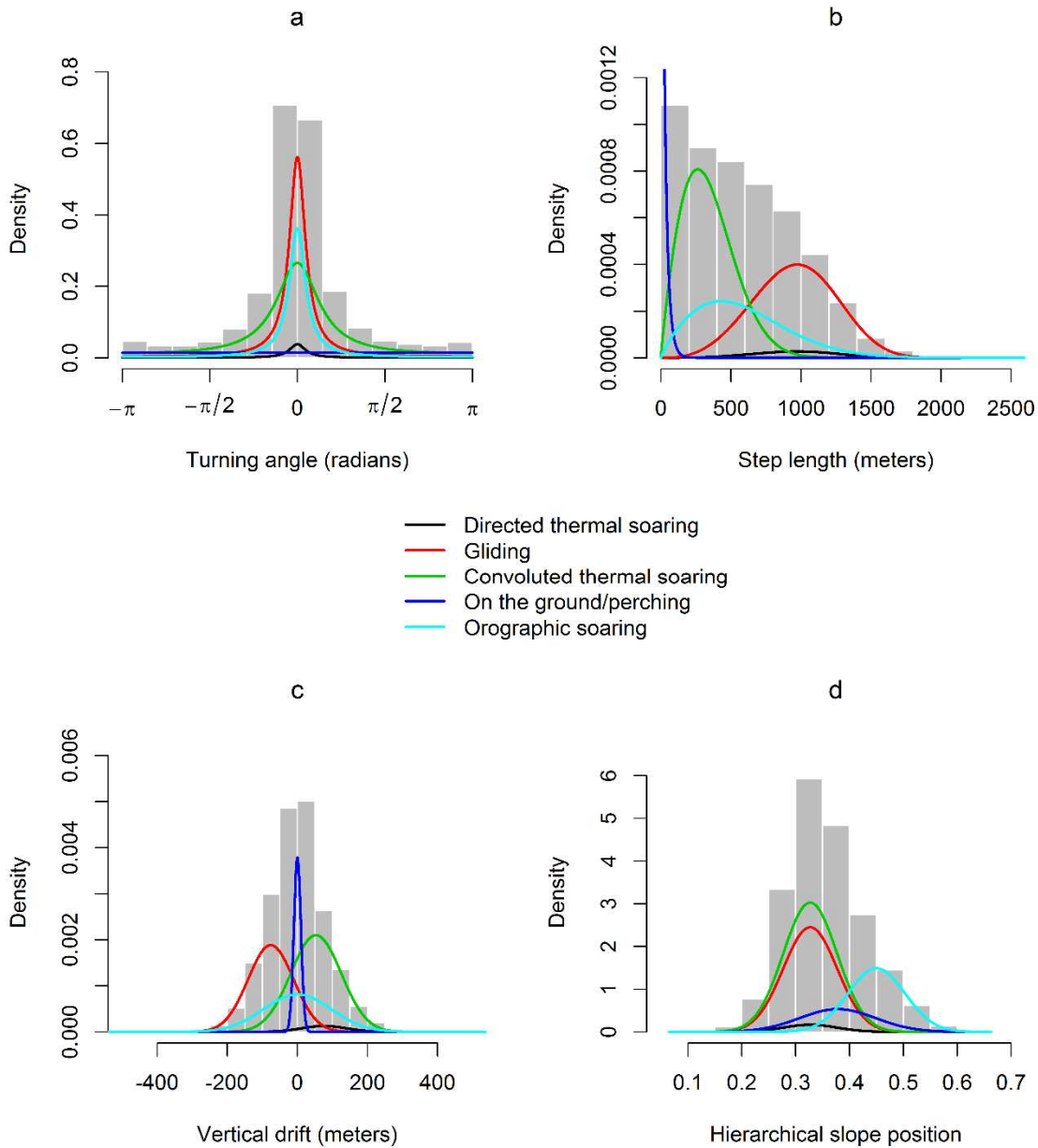
Figure S1. State-dependent emission distributions of the four response variables: a) turning angle, b) step length, c) vertical drift and d) hierarchical slope position, plotted over regularised data (grey histogram). To help visualisation, plots were truncated at 2000 m for step length and ±500 meters for vertical drift.
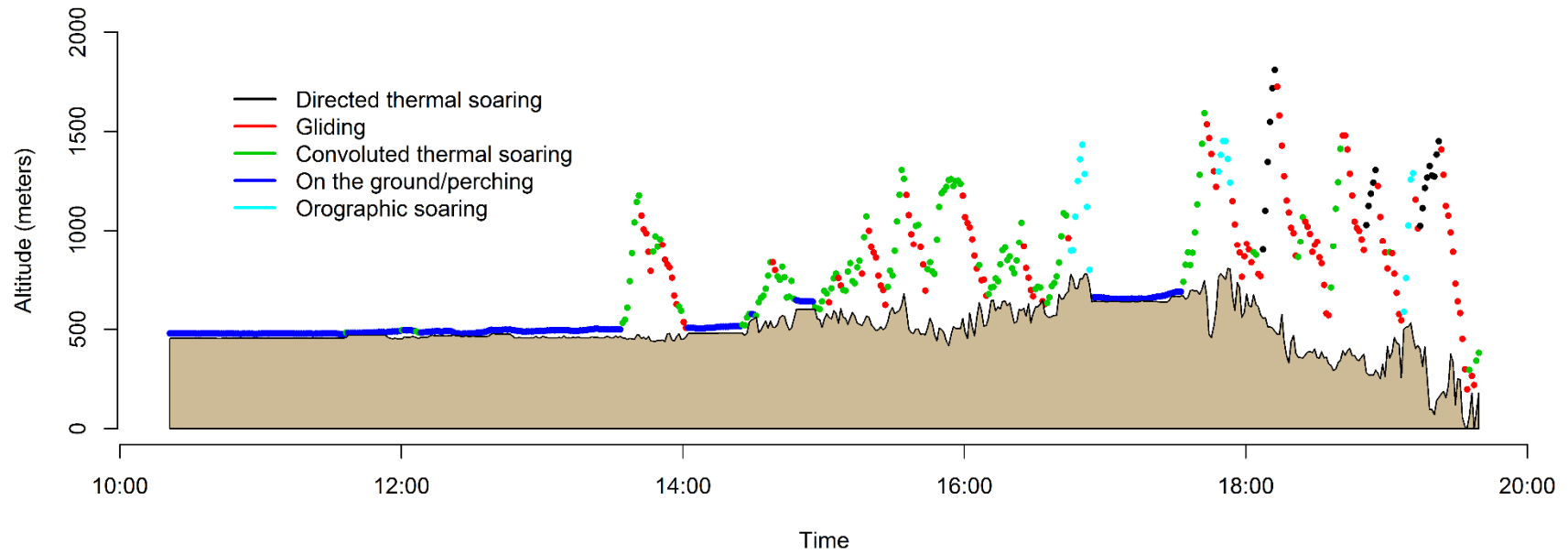
Figure S2. Example of time series of true altitudes from a track segment, coloured by the median posterior behavioural state at those locations. The filled polygon represents elevation at the corresponding GPS positions.

Table S4. Confusion matrix comparing manual state classifications (from Katzner et al., 2015) and model state estimates based on the posterior medians. Grey boxes highlight matching classifications.

Model → ↓ Manual	State 1 and 3 (thermal soaring)	State 2 (gliding)	State 5 (orographic soaring)	State 4 (on the ground or perching)	Accuracy
Thermal soaring	1660	438	374	4	**0.67**
Gliding	446	1766	308	1	**0.70**
Orographic soaring	134	114	464	2	0.65
Unknown	1497	289	294	27	-
Reliability	**0.44**	**0.68**	**0.32**	-	

Table S5. Results of model selection for the behavioural models, based on Akaike's information criterion corrected by small samples sizes (AICc). Best models (i.e. minimising the AICc) are highlighted in bold. The symbol '*' indicates the interaction between two variables.

Behavioural state	Data subset	Fixed effects	Random effects	AICc
Directed thermal soaring (State 1)	Adults and sub-adults; autumn and spring	~ Season * Age	Individual	772
			Year	902
			Individual, Year	548
		~ Season + Age	**Individual, Year**	**546**
		~ Season	Individual, Year	567
		~ Age	Individual, Year	672
	Adults; autumn and spring	~ Season * Sex	Individual	324
			Year	473
			Individual, Year	288
		~ Season + Sex	Individual, Year	288
		~ Season	**Individual, Year**	**285**
		~ Sex	Individual, Year	352
Gliding (State 2)	Adults and sub-adults; autumn and spring	~ Season * Age	Individual	961
			Year	1066
			Individual, Year	858
		~ Season + Age	**Individual, Year**	**856**
		~ Season	Individual, Year	858
		~ Age	Individual, Year	1041
	Adults; autumn and spring	**~ Season * Sex**	Individual	448
			Year	577
			Individual, Year	**411**
		~ Season + Sex	Individual, Year	462
Convoluted thermal soaring (State 3)	Adults and sub-adults; autumn and spring	**~ Season * Age**	Individual	854
			Year	1196
			Individual, Year	**805**
		~ Season + Age	Individual, Year	817
	Adults; autumn and spring	~ Season * Sex	Individual	457
			Year	606
			Individual, Year	460

		~ Season + Sex	Individual	455
		~ Season	**Individual**	**453**
		~ Sex	Individual	460
Orographic soaring (State 5)	Adults and sub-adults; autumn and spring	~ Season * Age	Individual	1548
			Year	1913
			Individual, Year	1364
		~ Season + Age	**Individual, Year**	**1362**
		~ Season	Individual, Year	1423
		~ Age	Individual, Year	1524
	Adults; autumn and spring	**~ Season * Sex**	Individual	773
			Year	859
			Individual, Year	**711**
		~ Season + Sex	Individual, Year	821

Figure S3. Dot plots of the random effects of individual and year in the final behavioural models. a-d) Results of the models assessing age and seasonal differences in the proportional occurrence of directed thermal soaring, convoluted thermal soaring, gliding and orographic soaring, respectively. f-e) Results of the models assessing sex and seasonal differences in the proportional occurrence of gliding and orographic soaring, respectively. All random effects are reported on the link scale (logit).
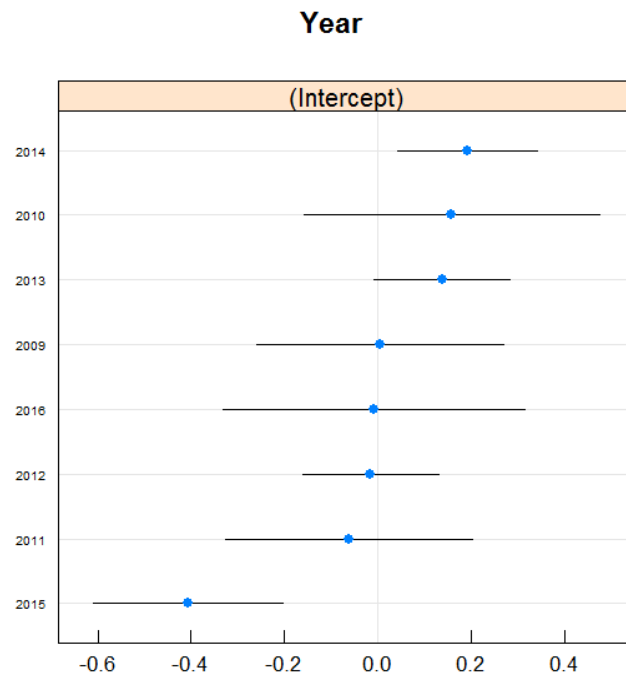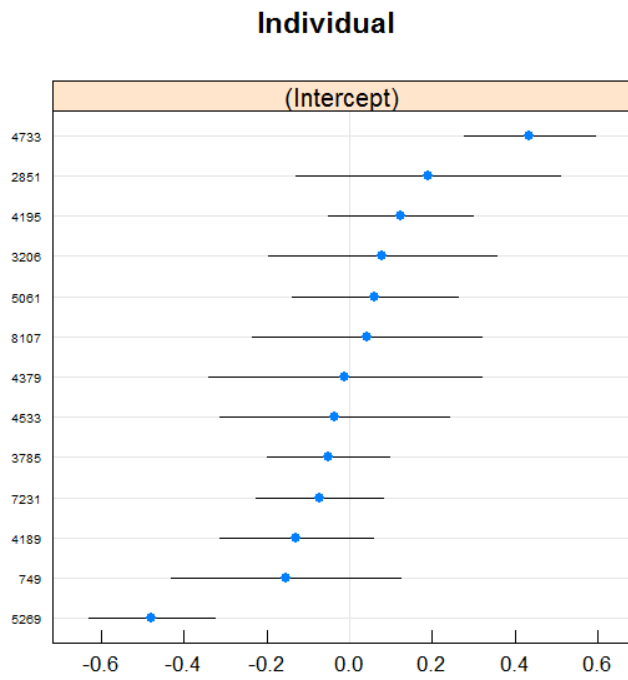
a)

b)

c)

d)

Individual

Year

(Intercept)

(Intercept)

e)
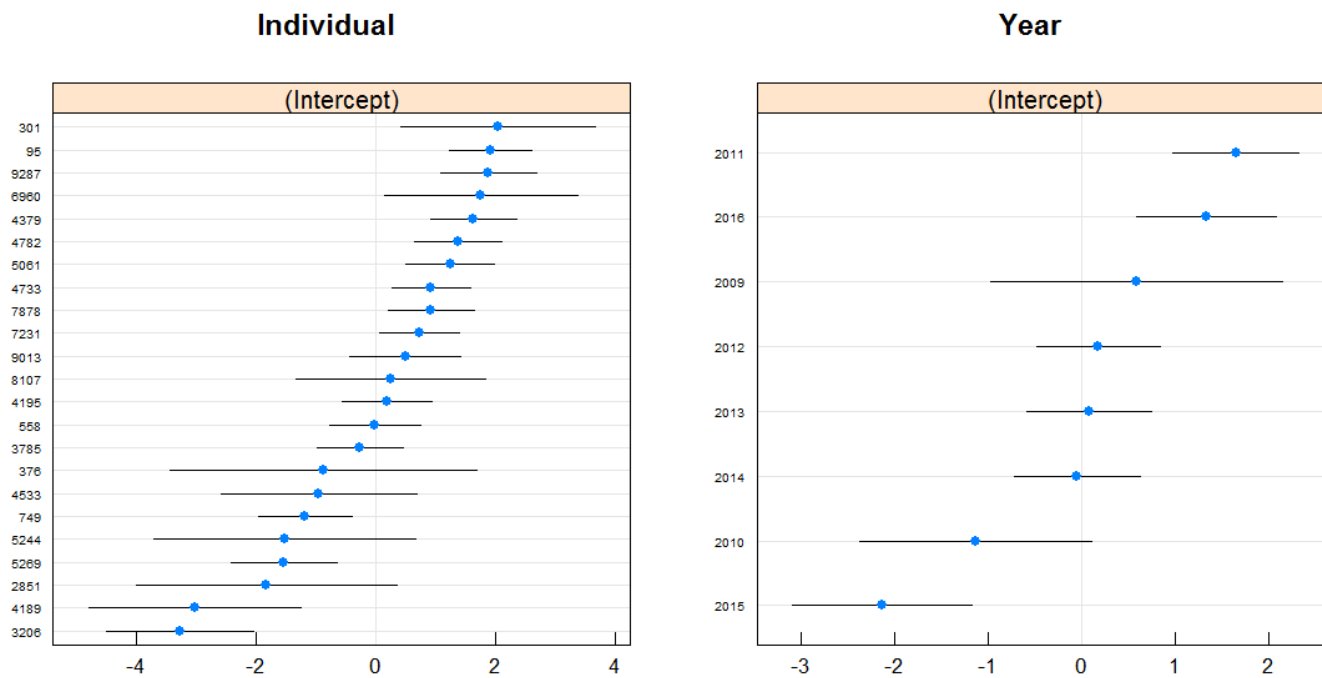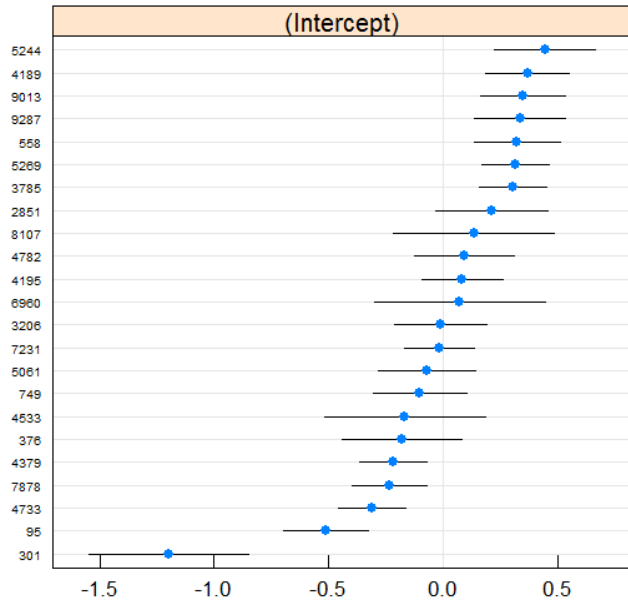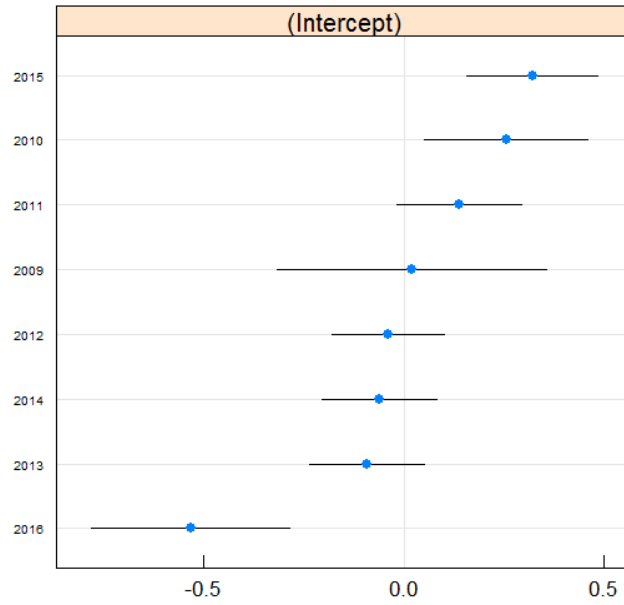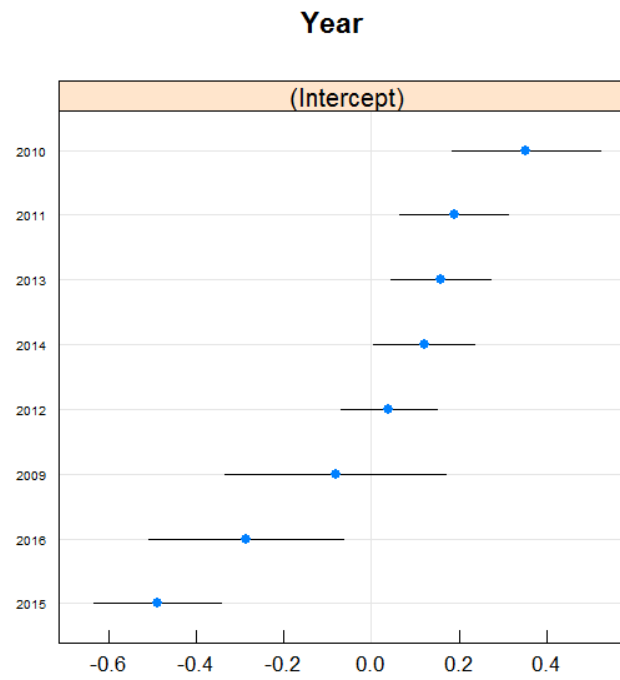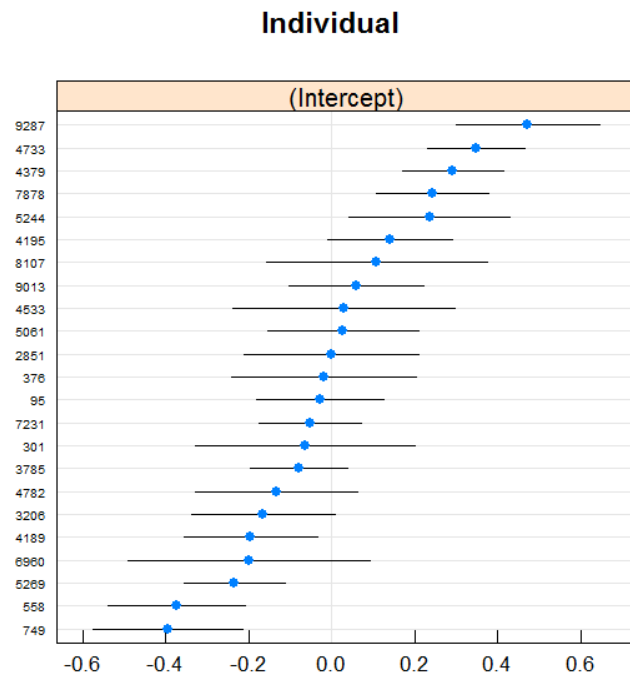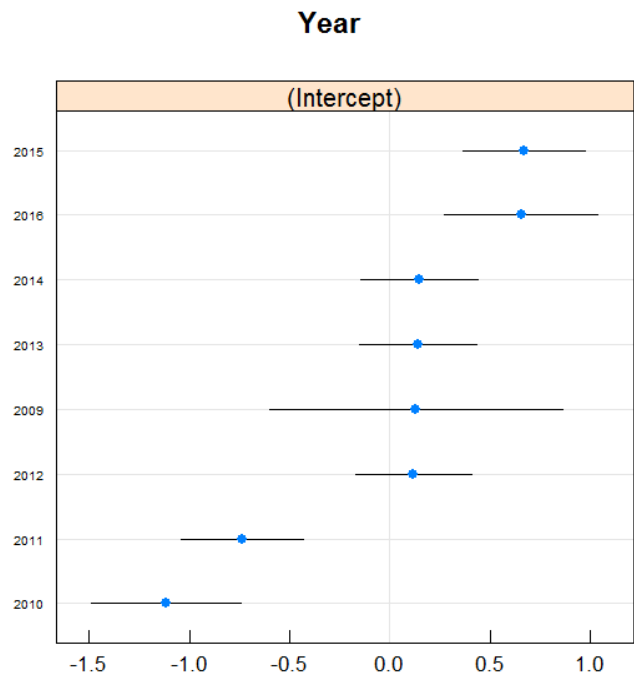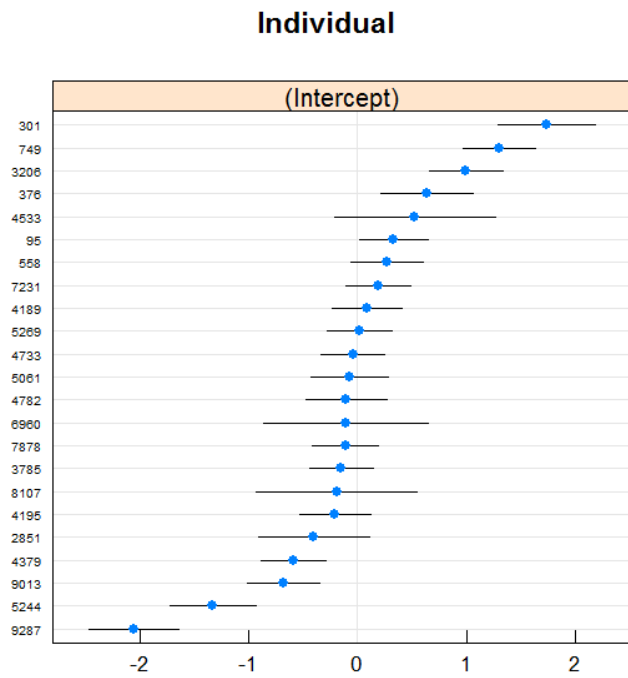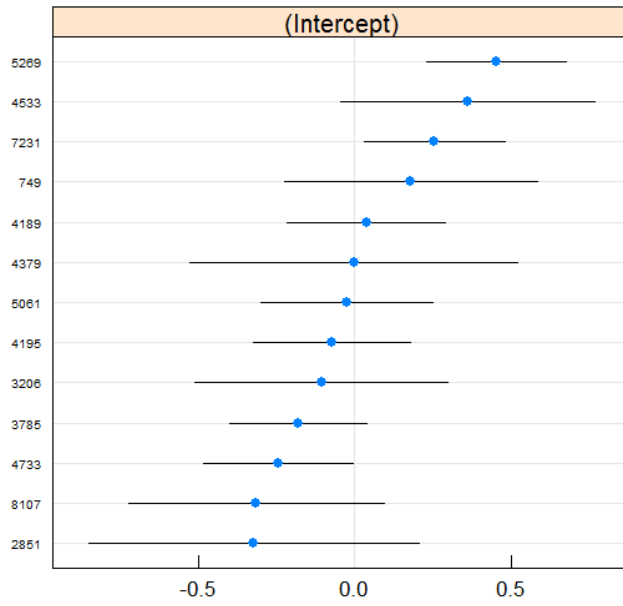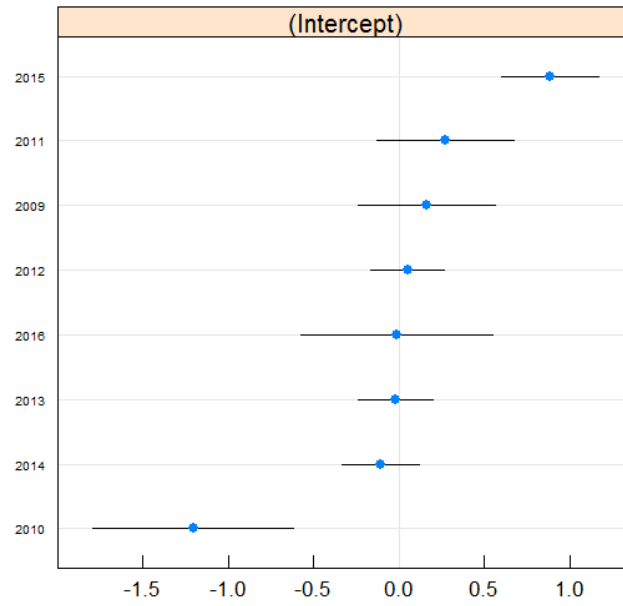
f)

Appendix S3. Reformulation of the model allowing for missing data.

The interpolation procedure used to fill any remaining, short (≤5 min) gaps in the observed track segments may introduce errors in the time series of response variables, particularly in the horizontal dimension. To test whether model results were affected by interpolated observations over these short gaps, the model was reformulated to allow for missing data points in the response variables. Specifically, whenever the time interval between a regularised location and the closest observed location was greater than 1 minute, rather than using the interpolated values of the response variables, the model was asked to estimate the missing values of the response variables, together with the rest of the parameters. When altitude information was missing at the second location of a segment (affecting the estimation of the vertical drift at the first location), a truncated Gaussian prior was provided, centred on the mean altitude for the corresponding segment, with a standard deviation of 2,000 m and truncation at the extremes of the observed altitude range.

The estimates of the parameters and associated uncertainty from this alternative version of the model are reported below. The 95% highest posterior density intervals for all parameters were largely overlapping between the two model formulations. As a result, the proportion of minutes classified under each latent state ($\delta_{1,\ldots,5}$) also remained largely unchanged in the new formulation.

Description	Parameter	Lower (2.5%)	Median	Upper (97.5%)
Vertical drift (altitude)	$\pi_1 = -\pi_2$	75	76	78
	π_3	52	53	55
Standard deviation (altitude)	$\sigma_1 = \sigma_2$	64	65	66
	σ_3	72	73	74
	σ_5	93	95	97
Concentration (turning angle)	$\rho_1 = \rho_2 = \rho_5$	0.83	0.83	0.83
	ρ_3	0.62	0.63	0.64
	ρ_4	0.00	0.00	0.00
Scale (step length)	$\alpha_1 = \alpha_2$	1061	1068	1075
	α_3	386	391	396
	α_4	22	23	24
	α_5	655	664	673
Shape (step length)	$\beta_1 = \beta_2$	3.57	3.62	3.68
	β_3	1.86	1.89	1.92
	β_4	0.90	0.92	0.95
	β_5	1.79	1.83	1.86
Mean (hierarchical slope position)	$\kappa_1 = \kappa_2 = \kappa_3$	0.326	0.327	0.328
	κ_4	0.376	0.378	0.380
	κ_5	0.448	0.450	0.451
Standard deviation (hierarchical slope position)	$\omega_1 = \omega_2 = \omega_3$	0.049	0.050	0.050
	ω_4	0.070	0.071	0.073
	ω_5	0.052	0.053	0.054
State proportions	δ_1	0.02	0.03	0.03
	δ_2	0.30	0.30	0.31
	δ_3	0.37	0.37	0.38
	δ_4	0.09	0.09	0.10
	δ_5	0.20	0.20	0.21
Transition probabilities	$\gamma_{1,1}$	0.752	0.784	0.814
	$\gamma_{2,1}$	0.012	0.015	0.018
	$\gamma_{3,1}$	0.001	0.002	0.003
	$\gamma_{4,1}$	0.000	0.000	0.001
	$\gamma_{5,1}$	0.000	0.000	0.001
	$\gamma_{1,2}$	0.170	0.200	0.232
	$\gamma_{2,2}$	0.711	0.720	0.729
	$\gamma_{3,2}$	0.174	0.181	0.188
	$\gamma_{4,2}$	0.000	0.000	0.001

	$\gamma_{5,2}$	0.058	0.064	0.071
	$\gamma_{1,3}$	0.000	0.001	0.006
	$\gamma_{2,3}$	0.217	0.225	0.234
	$\gamma_{3,3}$	0.779	0.787	0.795
	$\gamma_{4,3}$	0.029	0.035	0.043
	$\gamma_{5,3}$	0.020	0.024	0.029
	$\gamma_{1,4}$	0.000	0.001	0.004
	$\gamma_{2,4}$	0.000	0.001	0.002
	$\gamma_{3,4}$	0.010	0.012	0.014
	$\gamma_{4,4}$	0.937	0.945	0.952
	$\gamma_{5,4}$	0.016	0.019	0.022
	$\gamma_{1,5}$	0.004	0.013	0.026
	$\gamma_{2,5}$	0.034	0.039	0.043
	$\gamma_{3,5}$	0.015	0.018	0.021
	$\gamma_{4,5}$	0.014	0.019	0.024
	$\gamma_{5,5}$	0.885	0.892	0.899
Initial state probabilities	φ_1	0.005	0.020	0.042
	φ_2	0.089	0.153	0.222
	φ_3	0.381	0.452	0.519
	φ_4	0.102	0.132	0.164
	φ_5	0.197	0.241	0.287

Appendix S4. Analysis of simulated data.

In order to investigate whether irregular sampling (resulting in gaps in the tracking data) and measurement errors in the vertical and horizontal dimensions affected the ability of the model to estimate the parameters correctly, we explored the performance of the model by means of simulated data.

First, the posterior estimates of the parameters of the state-dependent emission distributions and of the transition probabilities were used to simulate thirty 10,000-minute-long time series of step length, turning angle, altitude and hierarchical slope position values. Specifically, the initial behavioural state for each track was set to 4 (i.e. on the ground or perching). A random value was then drawn from the posterior distribution of each parameter of the state-dependent emission distributions and of the corresponding transition probabilities. The set of transition probabilities was used to draw the behavioural state in the following time step, while the emission distributions were used to simulate a new value for each response variable. This was repeated 10,000 times for each simulated track. Errors in the vertical dimension were simulated using the same observation model used in the original analysis. We then extracted all gaps ≥ 2 min observed in the original data and distributed them randomly over the simulated data. Very large gaps (≥ 1 d) were excluded because they could not be placed randomly over the simulated tracks without generating extremely large tracks; however, this is unlikely to affect the outcome of the simulation procedure, because larger gaps would simply lead to the creation of additional segments. As described in the data processing section, we then divided tracks into separate segments whenever the gap was greater than 5 min, and interpolated the values of the response variables for shorter gaps. The first 7,000 observations of each track were discarded to: 1) avoid any influence of initial conditions; and 2) obtain a simulated tracking dataset of comparable size

to the original data. The final simulated dataset included 42,783 data points. We simulated errors in the horizontal dimension using a randomly sampled HDOP value from the original dataset: we drew a random value from a Gaussian distribution centred on the simulated step length, with standard deviation equal to the random HDOP value multiplied by the GPS error of the devices (3 m). Finally, we ran the state-space analysis on the resulting, simulated data, using the same priors and initial values as in the original analysis.

The estimates of the parameters and associated uncertainty from the analysis of the simulated data are reported below. With the exception of the initial state probabilities (which are necessarily different in the simulated data) and, to a certain extent, of the state proportions (reflecting the simulation ability of the model; see discussion in Appendix S5), the 95% highest posterior density intervals for all other parameters were largely overlapping between the analysis of observed and simulated data. These results suggest that the model is able to retrieve the correct parameter estimates despite observed gaps in the tracks and measurement errors.

Description	Parameter	Lower (2.5%)	Median	Upper (97.5%)
Vertical drift (altitude)	$\pi_1 = -\pi_2$	73	75	76
	π_3	51	53	54
Standard deviation (altitude)	$\sigma_1 = \sigma_2$	62	63	64
	σ_3	70	71	72
	σ_5	96	98	100
Concentration (turning angle)	$\rho_1 = \rho_2 = \rho_5$	0.83	0.84	0.84
	ρ_3	0.64	0.65	0.65
	ρ_4	0.00	0.01	0.02
Scale (step length)	$\alpha_1 = \alpha_2$	1055	1061	1067
	α_3	387	391	395
	α_4	24	25	25
	α_5	652	661	670
Shape (step length)	$\beta_1 = \beta_2$	3.57	3.63	3.68
	β_3	1.86	1.89	1.92
	β_4	0.96	0.98	1.00
	β_5	1.81	1.84	1.87
Mean (hierarchical slope position)	$\kappa_1 = \kappa_2 = \kappa_3$	0.326	0.327	0.327
	κ_4	0.375	0.377	0.379
	κ_5	0.449	0.450	0.451
Standard deviation (hierarchical slope position)	$\omega_1 = \omega_2 = \omega_3$	0.050	0.050	0.051
	ω_4	0.069	0.071	0.072
	ω_5	0.052	0.052	0.053
State proportions	δ_1	0.02	0.02	0.02
	δ_2	0.29	0.29	0.30
	δ_3	0.35	0.36	0.36
	δ_4	0.15	0.15	0.15
	δ_5	0.18	0.18	0.18
Transition probabilities	$\gamma_{1,1}$	0.702	0.741	0.778
	$\gamma_{2,1}$	0.014	0.018	0.021
	$\gamma_{3,1}$	0.001	0.003	0.004
	$\gamma_{4,1}$	0.000	0.000	0.001
	$\gamma_{5,1}$	0.000	0.001	0.003
	$\gamma_{1,2}$	0.190	0.226	0.265
	$\gamma_{2,2}$	0.711	0.721	0.730
	$\gamma_{3,2}$	0.171	0.178	0.186
	$\gamma_{4,2}$	0.000	0.001	0.003
	$\gamma_{5,2}$	0.059	0.065	0.072
	$\gamma_{1,3}$	0.000	0.005	0.020

	$\gamma_{2,3}$	0.216	0.224	0.233
	$\gamma_{3,3}$	0.782	0.789	0.797
	$\gamma_{4,3}$	0.032	0.037	0.042
	$\gamma_{5,3}$	0.020	0.025	0.030
	$\gamma_{1,4}$	0.000	0.001	0.007
	$\gamma_{2,4}$	0.001	0.001	0.002
	$\gamma_{3,4}$	0.011	0.013	0.015
	$\gamma_{4,4}$	0.937	0.943	0.949
	$\gamma_{5,4}$	0.016	0.019	0.023
	$\gamma_{1,5}$	0.013	0.025	0.041
	$\gamma_{2,5}$	0.032	0.036	0.040
	$\gamma_{3,5}$	0.014	0.017	0.019
	$\gamma_{4,5}$	0.015	0.019	0.023
	$\gamma_{5,5}$	0.881	0.889	0.897
Initial state probabilities	φ_1	0.006	0.010	0.032
	φ_2	0.254	0.323	0.398
	φ_3	0.276	0.346	0.417
	φ_4	0.100	0.128	0.159
	φ_5	0.154	0.191	0.233

Appendix S5. Posterior predictive checks.

Assessing the goodness-of-fit of hidden state models fitted in a Bayesian framework is less straightforward than in comparable frequentist models (Jonsen et al., 2013). Alternatively, posterior predictive checks can be used to assess the ability of the model to replicate various features of the observed data. De Haan-Rietdijk et al. (2017), Morales, Haydon, Frair, Holsinger, & Fryxell (2004), and Shirley, Small, Lynch, Maisto, & Oslin (2010) proposed several procedures to this purpose, which all aim to evaluate whether the simulation of new data using the posterior estimates of model parameters can generate summary statistics that are comparable with the same summary statistics in the empirical dataset.

We followed the procedure described in Appendix S4 to simulate 1,000 new datasets of comparable size based on random draws from the posterior distribution of the state-dependent parameters of the emission distributions and transition probabilities. By doing so, we implicitly accounted for uncertainty in these parameters. Results of the simulations were then compared to the dataset of filtered and regularised locations that was used to fit the model.

First, we compared the activity budget, i.e., the proportion of time spent in each latent state across all segments and tracks. The proportion of time spent in each state in the original data was plotted over the distribution of proportions obtained in the simulated datasets. Similarly, we calculated the mean and standard deviation of the duration of stays (i.e., the number of consecutive one-minute steps) in each state for each simulated dataset, and compared their distribution with the same statistics in the original data. We then considered the number of behavioural transitions per segment, corrected by the length of each segment. As for the previous metric, we plotted the mean and standard deviation in the original dataset over the distribution of the same statistics in the simulated dataset. Because the distributions of relative number of

behavioural transitions were not Gaussian and, therefore, the mean and standard deviation did not necessarily provide appropriate summaries as for the other metrics, we also plotted them together to verify their degree of overlap. Finally, we plotted the autocorrelation function plot (ACF) for all response variables in the original and simulated data.

The activity budget estimated from the simulated data was, overall, satisfactorily comparable with the activity budget in the original data (Fig. S4a). In the simulated tracks, eagles allocated more time than expected to state 4 (on the ground or perching), which also partially affected the proportional occurrence of other states. However, this could result from the fact that, at night or when not flying (that is, when an eagle is most likely to spend time in this state), the GPS device was programmed to record location data less frequently, resulting in a higher chance of gap occurrence; on the other hand, gaps were distributed randomly in the simulated data. This is also reflected in the higher mean duration of stays in this state in the simulated data (Fig. S4b). For all other states, the mean duration of stays in the original data was higher than in the simulated data, highlighting the potential problems with the validity of the Markov property for the short time interval that are discussed in the main text (Fig. S4b and c). Similarly, the relative number of behavioural transitions per segment was slightly higher in the simulated data (Fig. S4d). As demonstrated in the overlap between the two distributions, this reflects a lower occurrence of intermediate numbers of transitions, which could characterise longer stretches of tracks spent in given states. Finally, the ACF plots confirmed these patterns and highlighted the occurrence of residual autocorrelation in some response variables (particularly step length and hierarchical slope position) under specific states (Fig. S5).

Figure S4. Results of the posterior predictive checks. In all plots, the dashed red line indicates the value of the corresponding metric in the original data, while the black line reports the kernel density of the same metric across 1,000 simulated datasets. a) Activity budget, expressed as the proportion of time spent in each behavioural state (1-5); b) mean duration of stays (i.e., the number of consecutive one-minute steps) per state; c) standard deviation of the duration of stays per state; d) mean, standard deviation and overall kernel density (black: simulated data; red: original data) of the number of behavioural transitions per segment, corrected by the length of each segment.
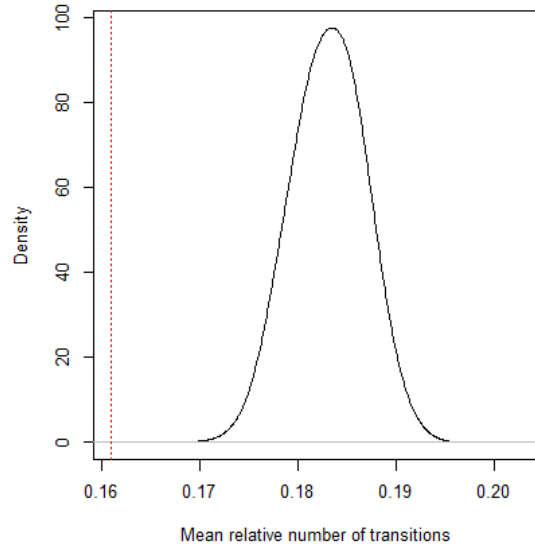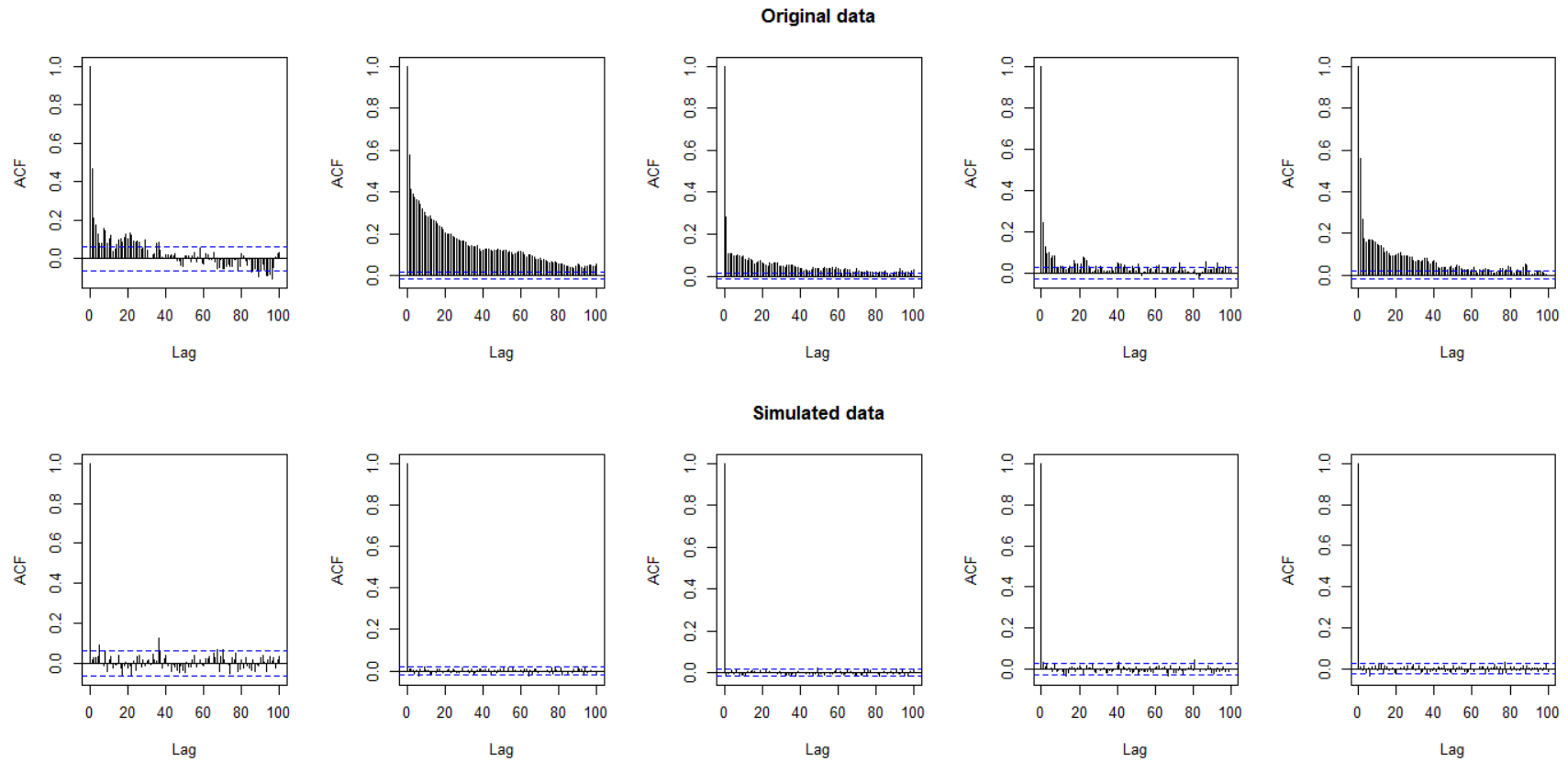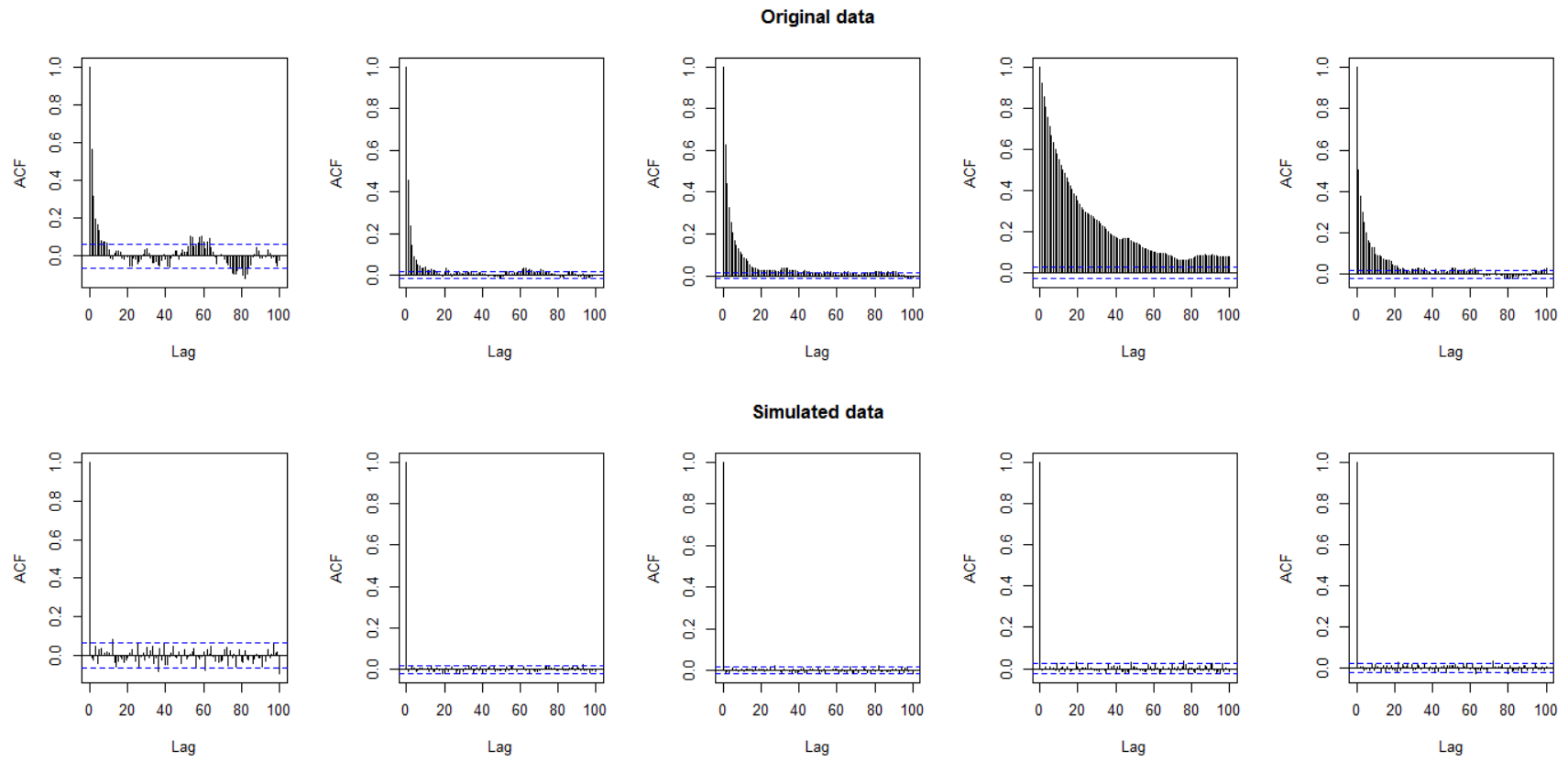
a)
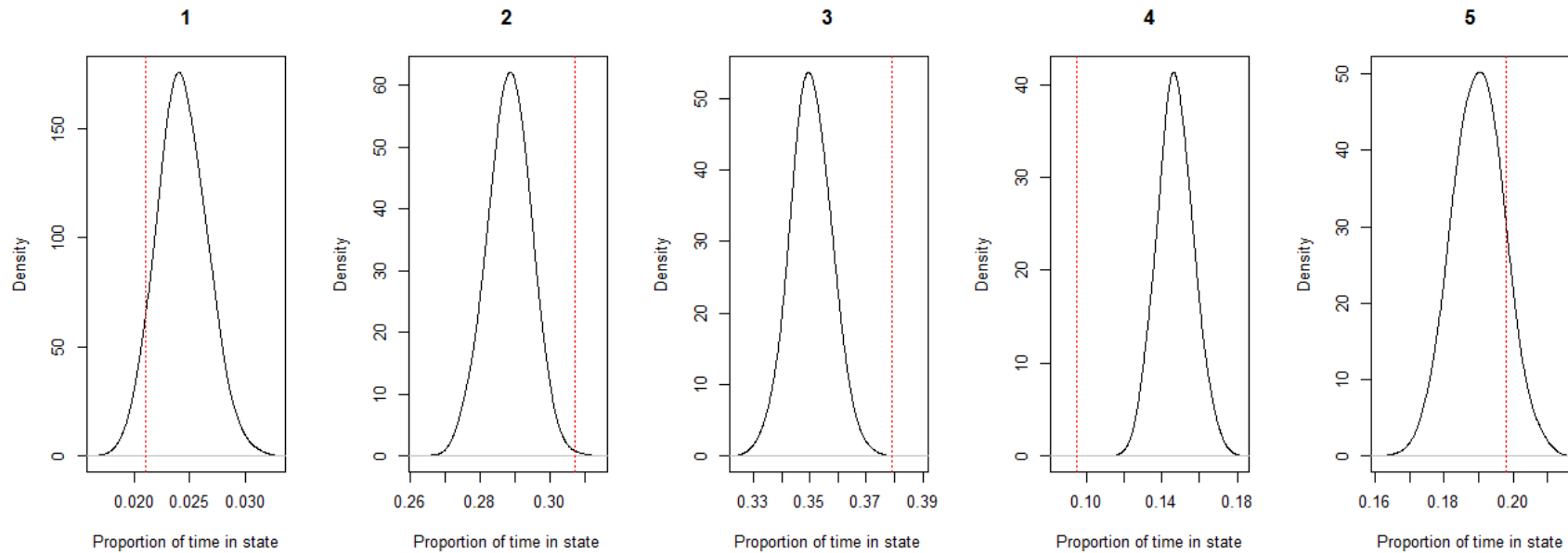
b)
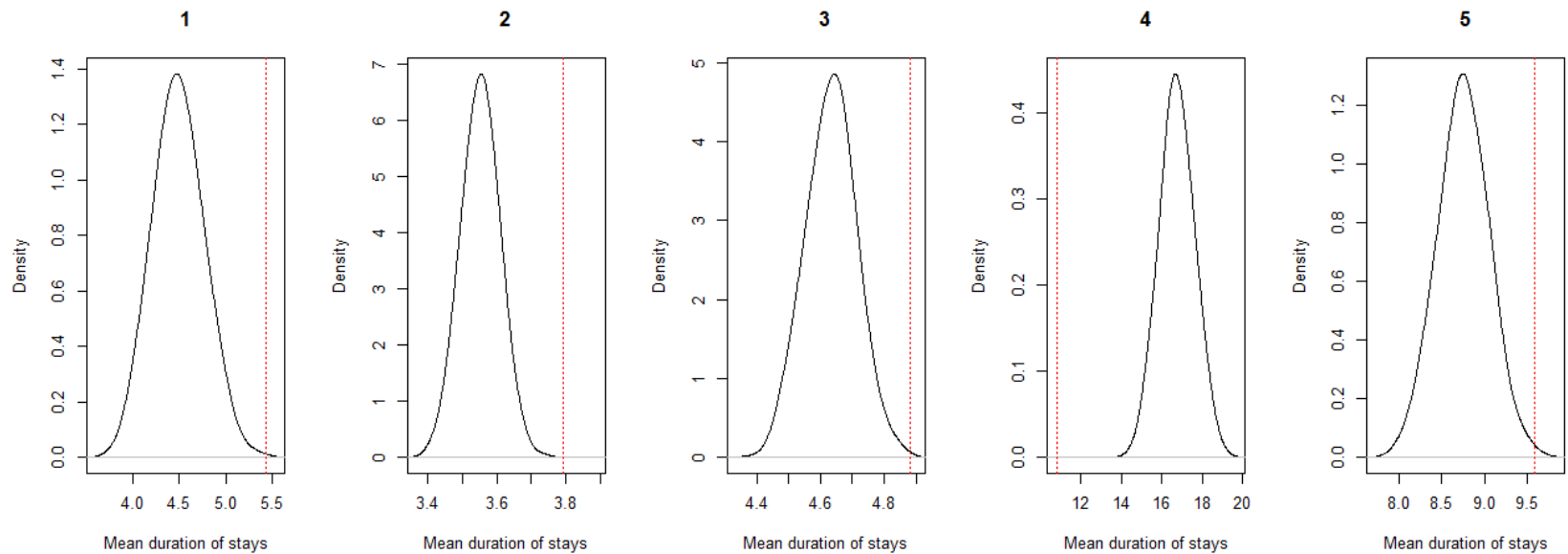
c)
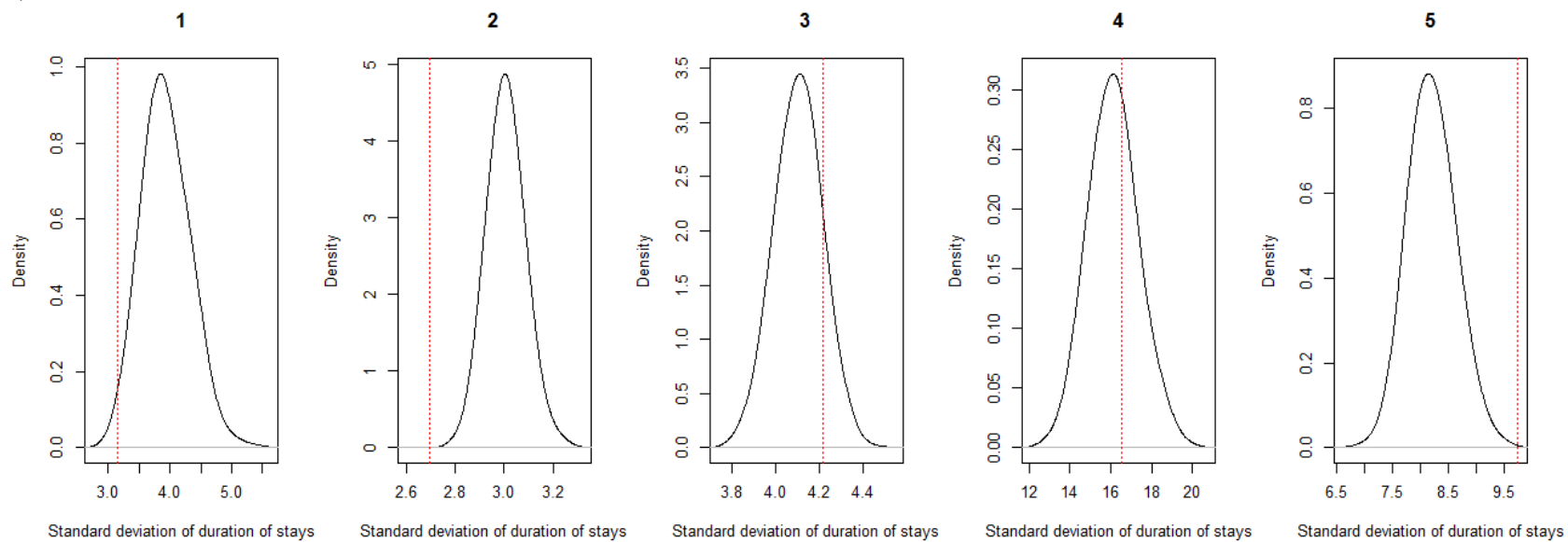
d)
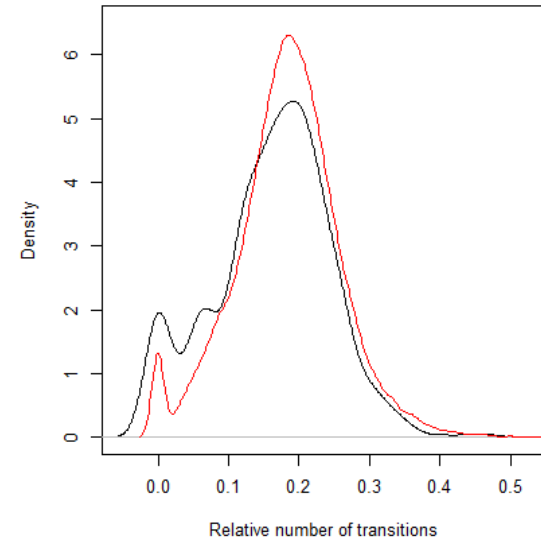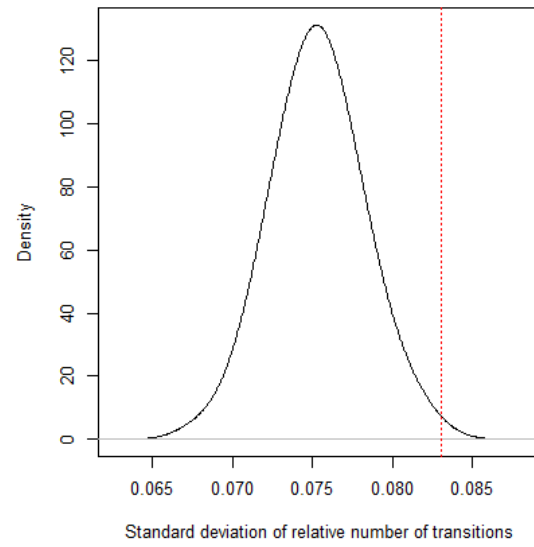
Figure S5. Autocorrelation function (ACF) plots for the response variables by state in the original and simulated data. a) Step length, b) turning angle, c) hierarchical slope position and d) vertical drift.
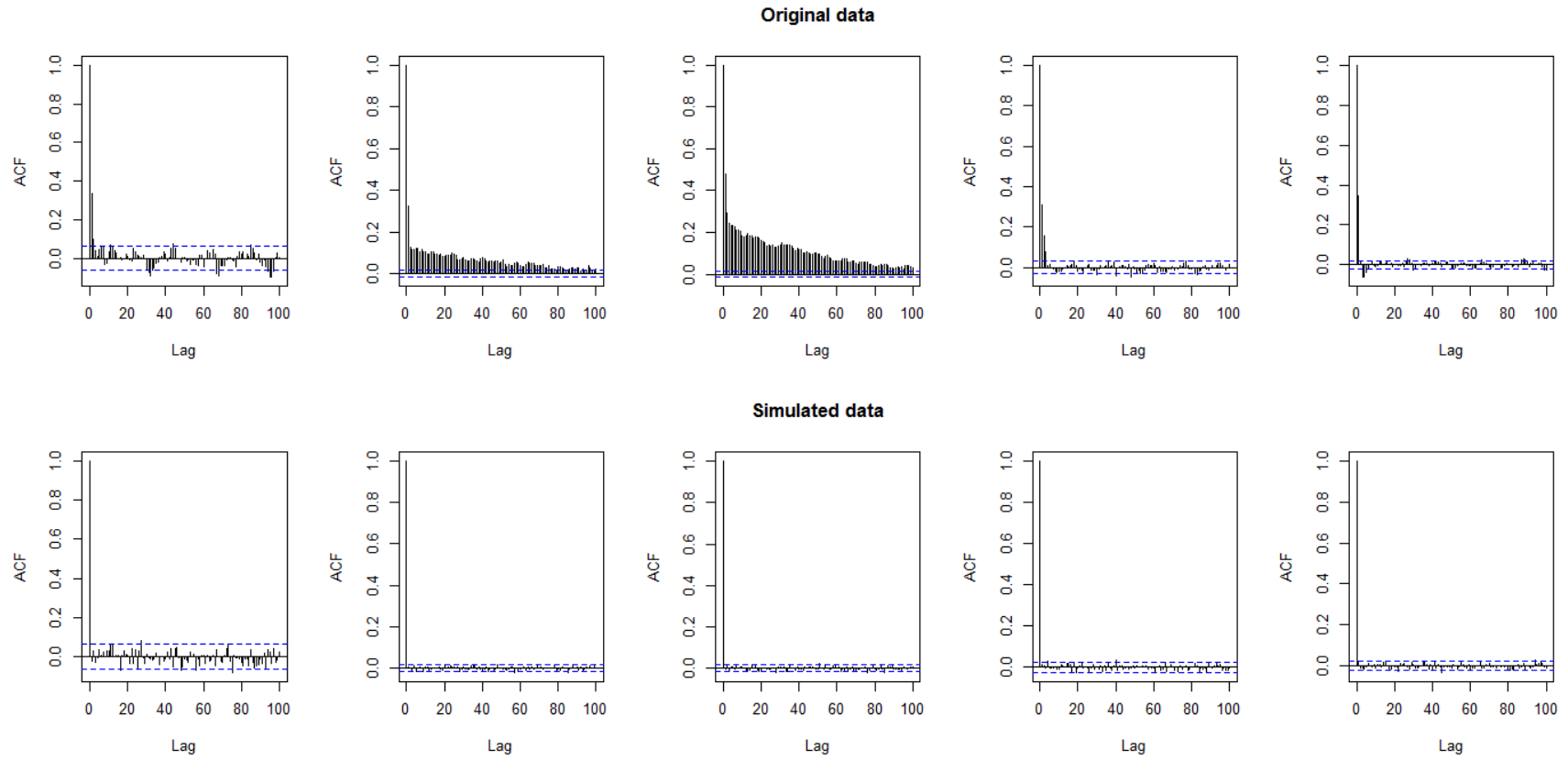
a)

b)

Original data

Simulated data

c)

d)

References

de Haan-Rietdijk, S., Kuppens, P., Bergeman, C. S., Sheeber, L. B., Allen, N. B., & Hamaker, E. L. (2017). On the Use of Mixed Markov Models for Intensive Longitudinal Data. *Multivariate Behavioral Research*, *52*(6), 747–767. doi:10.1080/00273171.2017.1370364

Jonsen, I., Basson, M., Bestley, S., Bravington, M. V., Patterson, T. A., Pedersen, M. W., … Wotherspoon, S. J. (2013). State-space models for bio-loggers: A methodological road map. *Deep Sea Research Part II: Topical Studies in Oceanography*, *88–89*, 34–46. doi:10.1016/j.dsr2.2012.07.008

Katzner, T. E., Turk, P. J., Duerr, A. E., Miller, T. A., Lanzone, M. J., Cooper, J. L., … Lemaître, J. (2015). Use of multiple modes of flight subsidy by a soaring terrestrial bird, the golden eagle *Aquila chrysaetos*, when on migration. *Journal of the Royal Society Interface*, *12*, 20150530. doi:10.1098/rsif.2015.0530

Lanzone, M. J., Miller, T. A., Turk, P., Brandes, D., Halverson, C., Maisonneuve, C., … Katzner, T. (2012). Flight responses by a migratory soaring raptor to changing meteorological conditions. *Biology Letters*, *8*(5), 710–713. doi:10.1098/rsbl.2012.0359

Morales, J. M., Haydon, D. T., Frair, J., Holsinger, K. E., & Fryxell, J. M. (2004). Extracting more out of relocation data: building movement models as mixtures of random walks. *Ecology*, *85*(9), 2436–2445. doi:10.1890/03-0269

Murphy, M. A., Evans, J. S., & Storfer, A. (2010). Quantifying Bufo boreas connectivity in Yellowstone National Park with landscape genetics. *Ecology*, *91*(1), 252–61. doi:10.1890/08-0879.1

Péron, G., Fleming, C. H., Duriez, O., Fluhr, J., Itty, C., Lambertucci, S., … Calabrese, J. M. (2017). The energy landscape predicts flight height and wind turbine collision hazard in three species of large soaring raptor. *Journal of Applied Ecology*, *54*(6), 1895–1906. doi:10.1111/1365-2664.12909

Shirley, K. E., Small, D. S., Lynch, K. G., Maisto, S. A., & Oslin, D. W. (2010). Hidden Markov models for alcoholism treatment trial data. *The Annals of Applied Statistics*, *4*(1), 366–395. doi:10.1214/09-AOAS282